Chapter 2

Citric Acid as a Precursor for Carbon Dots: Synthesis, Properties, Applications and Sustainability

Ricardo M. S. Sendão
José Pedro Silva
Martinho Freitas
Beatriz Azevedo Carneiro
Joaquim C. G. Esteves da Silva
and Luís Pinto da Silva[*]
Chemistry Research Unit (CIQUP), Institute of Molecular Sciences (IMS),
Department of Geosciences, Environment and Territorial Planning,
Faculty of Sciences, University of Porto (FCUP), Porto, Portugal

Abstract

Citric acid is a versatile weak acid compound that is best known for its role in the citric acid cycle, a process that occurs in the metabolism of all aerobic organisms. Citric acid is also employed in several other applications, including the synthesis of carbon dots (CDs). These carbonaceous nanoparticles present several interesting properties, such as a high photoluminescence, broadband absorption of light, biocompatibility, and low toxicity, making them good candidates for a wide range of applications.

CDs are produced following either top-down or bottom-up methodologies, with citric acid being commonly used as a carbon source

---

[*] Corresponding Author's Email: luis.silva@fc.up.pt.

In: Advances in Chemistry Research. Volume 79
Editor: James C. Taylor
ISBN: 979-8-88697-947-3

in the synthesis. Due to being inexpensive, readily available, and presenting the desirable characteristics for the synthesis, citric acid can easily be employed solo or in conjugation with heteroatom or metallic dopants to yield finely tuned CDs with the desired properties.

Herein, we will discuss the use of citric acid (both solo and in conjugation with dopants) for the synthesis of CDs, the particles resulting thereof, their applications and potential development of novel technologies. Furthermore, the effect role of the synthesis by-products on the citric acid-based CDs' properties and reactivity is also reviewed.

Finally, considering the importance of environmental sustainability of a process in today's world, the efficient substitution of commercial grade citric acid by biomass and waste products as carbon source for the synthesis is also reviewed, including the different environmental impacts that result thereof. The potential of carbon dots as catalysts for energy-efficient reactions, such as marine chemiluminescence, will also be reported.

Keywords: citric acid, carbon dots, sustainability, engineered nanomaterials, sensing, bioimaging, catalysis, fluorescence, chemiluminescence

Introduction

Citric acid (CA), also denominated as 2-Hydroxypropane-1,2,3-tricarboxylic acid is a colorless weak organic acid presenting the chemical formula $HOC(CO_2H)\ (CH_2CO_2H)_2$ (Figure 1). CA is naturally present in several fruits and vegetables, most important of which are citrus fruits (such as limes and lemons), from which its name is derived. In fruits with a high concentration of CA, it can constitute as high as 8% of the fruits' dry weight, with the concentration in the citrus fruits ranging anywhere between 0.005 M and 0.3 M for oranges and grapefruits, respectively [1]. The best-known application of CA is its role as an intermediate in the CA cycle, which is a part of the metabolism of aerobic organisms.

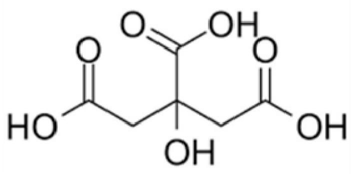

Figure 1. CA structure.

Regarding its general properties, CA is available in both as an anhydrous (MW = 192.123 g mol^{-1}) or as a monohydrate (MW = 210.140 g mol^{-1}), having the appearance of small-sized white or colorless crystalline structures. It is highly soluble in water (up to 64.3% w/w at 30ºC) and ethanol. CA solutions can be employed as buffer solutions between pH 2 and pH 8, whereas a 1 mM solution of the compound presents a pH of 3.2, explaining the acidity of citrus fruits, who tend to have a higher concentration of CA, and thus a lower pH.

Albeit naturally occurring, CA was not isolated until 1784, when it was crystallized from lemon juice. It took another century (1890) for it to be industrially produced, a process based in the citrus juice being mixed with calcium hydroxide to precipitate calcium citrate, which was then converted into CA via interaction with sulfuric acid. Three years later, another process, based on the microbial production of CA from sugar, was reported. The microbial pathway became the predominant CA production method, with the pharmaceutical companies Pfizer and Citrique Belge employing the mold *Aspergillus niger* in the large-scale production of CA. Thus, the major production route for CA was discovered and is still used to this day.

Cultures of *A. niger* are inserted into a sucrose or glucose-rich medium, feed on the sugars, and are then filtered [2]. After this, similar to the process first used in 1784, calcium hydroxide is added to precipitate citrate, which is turned into CA by reacting with sulfuric acid. In our age, it is estimated that over two million tons of CA are produced every year, with over half of the total production originating in China. The large amount is justified by the wide range of everyday applications. More than 50% of the total production is used in the beer industry as an acidity regulator, whereas an additional 20% is used in other food applications and other 20% in detergent applications. The remaining 10% of the production is for all the remaining applications, including its use in cosmetics, pharmaceuticals and in the chemical industry [3].

CA is required for many applications and processes, most important of which, the cyclic acid cycle, or Krebs cycle. This is of paramount important for aerobic organisms, the chains of reactions involved are responsible for around two-thirds of all food-derived energy obtained by complex organisms. However, CA is also important in processes outside the realm of biochemistry. Its major industrial application is in the food and beverage industry. Due to being one of the stronger, but edible, acids, it is commonly used as a flavoring and preservative in food and beverages, especially soft drinks and sugar-rich candies [3]. Due to CA being an excellent chelating agent, citrate salts of diverse metals are chosen as carriers to facilitate the uptake of these minerals by the organism. Moreover, CA is also used as an emulsifying agent in ice cream and caramel and is even employed as a substitute of lemon juice and vinegar in some recipes.

Outside the food and beverage industry, it is used for purposed as varied as the making of bath salts and bombs, shampoos, a degreasing agent, removal of limescale from boilers, water treatment via metal removal, rust removal, stainless steel passivation, soldering flux and production of antiviral facial tissues. Finally, being a versatile precursor to several organic molecules, it is also employed in the chemical industry. This chapter concerns a particular application of CA, its use as a carbon source in the fabrication of carbon-based nanoparticles, also known as carbon dots (CDs).

Carbon Dots: What Are They?

Over the past few years, nanostructured materials have been extensively studied as potential substitutes to traditionally used materials. Due to the properties enabled by their nanosized structure, these materials present superior properties for a whole range of applications. Regarding a particular nanomaterial class, carbon-based nanomaterials, several subtypes of nanomaterials have been added to the family over the years, each presenting their own unique properties and advantages. Carbon is a black material that, when in bulk, is not soluble in water and is not able to present photoluminescence. However, when in a nanosized form, it displays properties that are largely different from those of the bulk material. These nanosized materials, suitable for a diverse range of applications, include both single [4] and multi-walled [5] carbon nanotubes, nanodiamonds [6], nanofibers [7], graphene [8], buckminsterfullerene [9], and CDs [10-15].

CDs were first discovered in 2004 by Xu et al., who, during the synthesis of single-walled carbon nanotubes, managed to isolate carbon nanoparticles as a by-product [16]. This novel class of carbon-based nanomaterials were named as CDs in 2006 by Sun et al., [17] becoming a topic of interest for the scientific community ever since. CDs are usually sized between 1 and 10 nm and display a spherical or near-spherical shape [18]. They may have a sp^2-conjugated amorphous or nanocrystalline core (depending on the synthetic methodology) with oxygenated functional groups on the surface, such as -OH, -COOH and -CHO [18, 19].

The CDs core is mostly made of sp^2-carbon or graphene/graphene oxide sheets interconnected by sp^3 carbon atoms located in-between the layers, forming a diamond-like array [20, 21]. On the surface level, several functional groups may be found (e.g., alcohols, amines, and carboxylic acids). These groups contribute to the CDs superior water solubility and allow the CDs to undergo additional functionalization and passivation steps (to enhance the CDs properties), as they provide binding sites for other molecules [20]. All this leads to a highly complex internal and external nanoparticle structure, whose constitution depends on the precursors and conditions used during the synthesis, both of which can be controlled and tuned to obtain the desired outcome.

From their structure results that CDs possess several desirable properties and characteristics, including its production being inexpensive, presenting a high photoluminescence quantum yield (QY_{PL}) [12, 13, 19, 22], broadband absorption range [20], good water solubility [12, 18], high photo- and chemical stability [18, 23], biocompatibility [9, 24, 25], and low toxicity [25, 26]. Moreover, when compared to their most direct competitors, metal-based quantum dots, CDs are considerably less toxic (due to not using heavy metals that are prone to cause bioaccumulation) and present a larger Stokes shift, meaning that the fluorescence wavelength maximum of the CDs can vary greatly depending on the excitation wavelength, which is contrary to what happens with quantum dots [23]. From this results that, for CDs, a variation of the excitation wavelength causes a shift of the emission spectrum and that if the nanoparticles' synthesis and post-synthetic treatment are performed properly, it is possible to obtain emissions in the near infrared region upon absorption of ultraviolet radiation [24].

Finally, there is also the possibility of fabricating CDs with up-conversion photoluminescence, something which allows the CDs to convert lower-energy higher-wavelength radiation into higher-energy lower-wavelength radiation, widening the potential uses of CDs and increasing their effectiveness in applications such as photocatalysis [27]. Considering the diverse properties displayed by CDs and the interest they might create for diverse applications, CDs usually need to be thoroughly characterized via techniques such as TEM/SEM, UV-Vis and photoluminescence spectroscopy, FTIR and XPS, among others.

CDs: Synthesis and Purification

Regarding their production, CDs can be prepared via an array of methodologies that can be separated into two main groups: top-down and bottom-up methodologies (Figure 2). Top-down methodologies are based on the CDs being prepared by breaking down bigger, macroscopic, bulk carbon materials, such as activated carbon, graphite, and carbon nanotubes. Usually, this requires expensive equipment and work-intensive techniques. This group includes the preparation of CDs via techniques such as arc-discharge [16], laser ablation [17], chemical exfoliation [28], ultrasonic treatment [29] and electrochemical shocking [30].

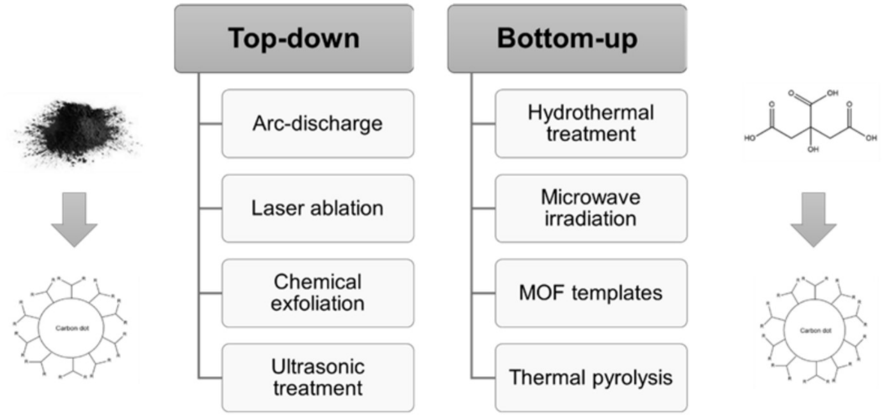

Figure 2. Top-down and bottom-up synthetic pathways to produce CDs.

Opposite to this we have bottom-up methodologies, which are based in the association of smaller, molecular-sized, carbon-based compounds (e.g., glucose and CA) into bigger structures, the CDs. Bottom-up methodologies include hydrothermal treatment [31-33], microwave irradiation [22, 31, 34, 35], metal-organic framework templates [36], plasma treatment [37] and thermal pyrolysis [38]. While each methodology has its merits and demerits, bottom-up routes are typically simpler, less expensive and faster than top-down routes. Because of this, typically bottom-up strategies are preferred in detriment of top-down routes. Across the variety of possible synthetic pathways, the most commonly employed routes for the synthesis of CDs are based in the microwave irradiation or hydrothermal treatment of a solution containing a molecular carbon-source, and, if doping the CDs is intended, heteroatom-containing compounds (typically nitrogen and Sulphur-sources) can be added to the precursor solution [22, 24, 27, 31-35, 39-42].

The first report concerning CDs produced via microwave irradiation came from Zhu et al., who in 2009 produced the carbon nanoparticles from a solution of poly(ethylene glycol) (PEG-200) and glucose/fructose [35]. A microwave oven was employed to irradiate to solution for 2 to 10 minutes (potency of 500W), after which resulted CDs ranging from 2.57 ± 0.45 to 3.65 ± 0.60 nm in diameter [35]. The CDs presented a high QY_{PL}, a broad absorption range (from the UV into the infrared), a high oxygen content and hydrophilic groups that permitted a superior water solubility, a characteristic trait of this kind of synthesis [35, 43, 44].

As for the hydrothermally synthesized CDs, the first ones were reported by Yang et al. in 2011 [45]. A mixture of glucose and potassium phosphate was prepared, dissolved, and transferred into a Teflon-lined autoclave. It was then subjected to a temperature of 200ºC for 12 h, after which a centrifugation and salt removal steps ensued [45]. By managing the molar ratios between the species in the precursor mixture, the authors obtained CDs with tunable emission and particle sizes, allowing for the making of tailor-made CDs for specific applications. The possibilities were nearly endless, as CDs with emissions across the whole visible range were produced [45].

Due to the easiness and low-cost of bottom-up strategies, in particular when compared to top-down methods, and due to the tunable emission properties of CDs, strategies such as hydrothermal treatment and microwave-assisted synthesis are regarded as the most commonly used ways of fabricating tailor-made CDs. Furthermore, with bottom-up strategies, when employing natural bioresources, it is possible to avoid the need of passivating the CDs surface, as -OH groups are already oxidized during the process, thus permitting a one-step synthesis of ready to use CDs while also reducing the cost in terms of time and resources [46, 47].

Finally, to obtain the CDs' carbogenic core, a carbon-source must always be used to provide the required components. Whereas CDs can derive from a variety of different precursors, both commercially available chemical reagents and natural resources (e. g. corn stover, bee wax, fish scales, among others), the most commonly employed carbon-source in CDs synthesis is CA. This reagent, which is inexpensive and easy to obtain, has been used in a multitude of CDs synthesis since they were discovered, as it possesses both carbon and oxygen atoms, is easily soluble and is known to produce highly photoluminescent CDs via both top-down and bottom-up synthetic methodologies.

Moreover, to further enhance the optical properties of the resulting nanoparticles, researchers frequently resort to heteroatom doping, a process in which a heteroatom containing molecule (e.g., urea or ethylenediamine for N-doping or thiourea for N,S-doping) is added to the reaction mixture [43, 48].

This requires a good interaction between the carbon source and the heteroatom containing molecules. CA, due to its chemical structure, can easily interact with heteroatom-containing groups such as amines, promoting the formation of citrazinic acid and its respective derivatives, which are strongly emissive blue fluorophores [49-51].

CA-Based CDs: Applications

Since their discovery, CDs have been used in several applications (Figure 3), even some for which quantum dots are unsuitable because of their toxicity. Thus far, the use of CDs has been reported for bioimaging [24, 52], sensing and biosensing [12, 32, 53], drug delivery systems [26, 54], photodynamic therapy [55, 56], nanothermometry [15], light emitting devices [57, 58], photocatalysis [10, 11, 59], and photovoltaic devices [60, 61], just to name a few. It is unsurprising that CA, being such a common carbon-source for CDs, was already used in nearly all of these applications. A brief paragraph on each main application is given below.

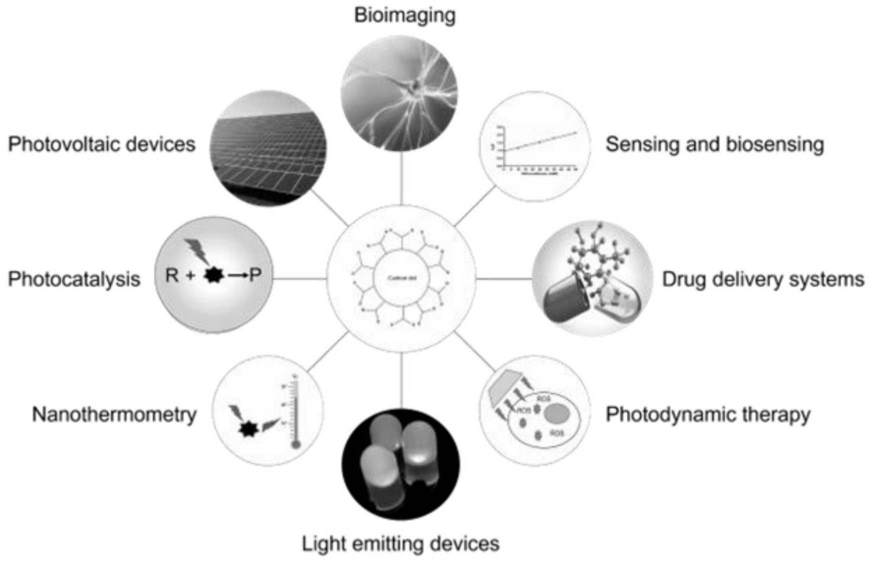

Figure 3. General representation of several applications for CDs.

Bioimaging

The low toxicity and high biocompatibility of CDs makes them good candidates for bioimaging, as their high photoluminescence permits an easier detection of the particles inside the study object. Fiori et al., using a hydrothermal route, prepared CDs from a combination of CA and either tris (hydroxymethyl)-aminomethane (tris) or arginine methyl ester dihydrochloride [62]. When characterized, the CDs made from CA and tris presented an average size of 2 nm, a high photostability and a QY_{PL} of 37%. Furthermore, the CDs proved to be biocompatible, allowing for a 100% cell survivability rate after 24 h of incubation [62]. Cell imaging tests confirmed the uptake of the CDs by the tested cells, with the CDs being mainly localized in the cytoplasm and occasionally in the nucleus.

Overall, the low cytotoxicity, high photoluminescence and easy uptake by the cells make these CDs potential candidates for application in bioimaging without risking damaging the targeted cells [62]. The previous work being just one example, more study cases can be found regarding successful CA-based CDs in bioimaging with other precursors: CA and ethylenediamine by Ding et al. [63], CA and tetraoctyalammonium bromide by Bhaisare et al. [64], CA and metformin by Wan et al. [65], CA and 8-aminiquinol by Li et al. [66], and CA and polyethylene imine by Wang et al. [67], just to name a few.

Sensing and Biosensing

Several cases have been reported on the successful use of CA-based CDs for both sensing and biosensing. Shan et al. [68] developed CA and benzoylurea-based CDs for the selective sensing of Fe(III). The CDs were prepared via calcination and presented an average size of 5.2 nm and a high, excitation-dependent, photoluminescence. In the presence of Fe(III), the CDs photoluminescence suffered quenching, allowing for a quantitative sensing of species with a detection limit as low as 1.1 µM. Furthermore, of 20 tested metal ions, only Fe(III) could quench the CDs' photoluminescence, indicating a high selectivity, which is important for sensing applications [68].

In another study, Wang et al. prepared CA and 3,5-diaminobenzoic acid-based CDs for the sensing of NO_2^- and pH on living cells [69]. The hydrothermal synthesis resulted in CDs with an average size of 2.16 nm, broad absorption, a high QY_{PL} of 41%, and more importantly, a low toxicity which enabled their use in biological samples. NO_2^- and pH sensing were achieved in HeLa cells using the CDs. Increasing NO_2^- concentrations and pH led to a quenching of the CDs' photoluminescence [69]. Other cases were reported for the sensing of both metals [70-72] and organic compounds [73-75] using CA-based CDs.

Drug Delivery Systems

The biocompatibility and molecular binding spots of CDs enable them to become potential drug delivery systems capable of transporting a coupled pharmaceutical into the target site (e.g., by easing their passage through the blood brain barrier).

Kong et al. reported the preparation of CA and ethylenediamine-based CDs via hydrothermal treatment towards the delivery of doxorubicin to the target site in breast cancer cells [54]. The prepared CDs were biocompatible and presented a quasi-spherical morphology with an average size of 0.5 nm. A quenching of the CDs' photoluminescence intensity confirmed the successful electrostatic-driven loading of doxorubicin onto the nanoparticles. A doxorubicin capacity of 28.75 mg g^{-1} was achieved with the CDs, with a release rate of 71% after 72 h at pH 7.4 (physiological levels) [54].

In terms of anti-tumoral efficiency, due to a higher degree of drug uptaking by the cell, doxorubicin-loaded CDs showed more cytotoxicity towards MCF-7 breast cancer cells than free doxorubicin. This was due to more doxorubicin being delivered to the drug target site with the complex, in this case, the cell nucleus [54]. Other examples of CA-based CDs for drug delivery systems can be found on [76-79].

Photodynamic Therapy

Good biocompatibility and low toxicity towards healthy human cells are known properties of CDs. However, in specific cases under suitable light irradiation, CDs are capable of a localized toxic effect by producing ROS when photoexcited, hence presenting potential for photodynamic therapy. In 2022 Suner et al. reported producing CA, ethylenediamine and arginine-based CDs via microwave-assisted synthesis [80]. The CDs presented an average size of 2.3 nm, a graphitic structure and high photoluminescence.

Their biocompatibility was confirmed via cytotoxicity analysis and blood compatibility tests. When excited under UV-light (315-400 nm, 300 W lamp), a 5 mg mL^{-1} concentration of CDs inhibited circa 49 ± 7% of the tested bacteria (*E. coli*) within 5 minutes of irradiation [80]. Other studies regarding the use of CDs for photodynamic therapy were reported for both microorganisms [81, 82] and tumor cells [83, 84].

Light Emitting Devices

Due to their high photoluminescence, tunable emission and photostability, it is no surprise that CDs have been studied for applications in light emitting devices. Wang et al. reported the microwave-assisted fabrication of CA and cyclen-based CDs for white light-emitting diodes [85]. The synthesized CDs, sized between 1 and 4 nm, presented an intense yellow solid-state fluorescence under UV-light and a QY_{PL} of 48%. However, when the excitation wavelength is changed to 450 nm, the CDs' emission peak is located at 546 nm (CIE coordinates 0.43, 0.55). This enables them to, when combined with a blue-emitting chip, to fabricate low-cost, non-toxic, and environmentally friendly white light-emitting diodes [85].

This is quite significant, as the current alternative for white light-emitting diodes is based on the use of semiconductor quantum dots, which use toxic heavy metals, and rare earth-based phosphors, which are both expensive and non-renewable. Other examples regarding the use of CDs for light-emitting applications can be found on [86-88].

Nanothermometry

One of the many possible operating principles behind nanothermometry is that of non-contact luminescent thermometry, which exploits temperature-dependent emissive behaviors as a base for temperature determination, a characteristic which CDs may present.

Kalytchuk et al. fabricated a nanothermometer out of CA and cysteine-based CDs prepared via hydrothermal treatment [15]. The particles displayed an average size of 4.5 nm, a stable photoluminescence, low toxicity, and good biocompatibility. Their photoluminescence lifetime is stable across different concentrations, ionic strengths, and pH values. Their photoluminescence lifetime was stable over 40 h, and sensible to temperature changes between 15 and 45 ºC.

Furthermore, this was reversible for at least 7 cycles, confirming its reusability and they presented a sensitivity of 1.79% K^{-1}. Due to their low cytotoxicity, high stability at biological pH and temperature ranges, high sensitivity to relevant temperatures, the CDs have potential for use in applications related to temperature measurements in biological samples [15]. Other examples of CA-based CDs exist for this application [89-91].

Photocatalysis

CDs are potential candidates for applications in photocatalysis due to their broad absorption range, photostability and capacity of generating charge carriers (e^- and h^+) upon suitable light absorption. In fact, they have been used for varied photocatalytic applications such as hydrogen generation via water splitting, photodegradation of organic pollutants and photoreduction (Figure 4) [92].

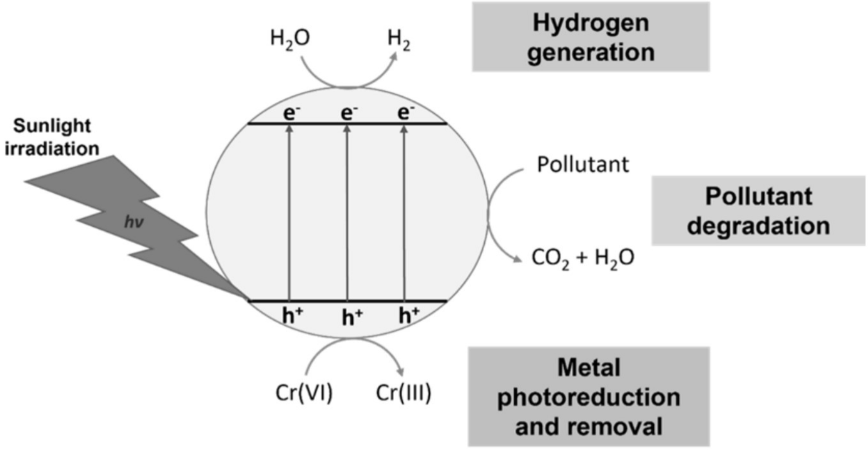

Figure 4. Possible application of CDs in photocatalysis. Reproduced with authorization from [92].

Jana et al. achieved efficient hydrogen generation using CA and urea-based CDs [93]. The CDs were prepared using a microwave-assisted method and presented sizes between 2.5 and 3.5 nm and potential for photoinduced electron transfer (PET). Under Xe lamp irradiation the best performing CDs achieved a maximum turnover frequency (TOF) of 15.15 mmol (H_2) g(CD2)$^{-1}$ h^{-1} after 1 h, which is comparable to that of most semiconductors [93].

Regarding pollutant degradation, Zhou et al. prepared gel-like CDs from CA and ethylenediamine towards the sunlight-driven degradation of common organic dyes [94]. The CDs managed to fully degrade the pollutants methylene blue, methyl orange and rhodamine B in 20, 40 and 60 minutes, respectively [94]. The use of CA-based CDs has been studied for hydrogen generation [95, 96], photodegradation [41, 97] and photoreduction [98, 99].

Photovoltaic Devices

Due to their properties, CDs are interesting study cases for application in photovoltaic devices. Lim et al. prepared CA and ethylenediamine-based CDs to be employed as an interlayer on photovoltaic devices [100]. The microwave-assisted synthesis yielded CDs with an average size of 10 nm. After synthesis and purification, they were then dispersed by spin coating on an ethoxylated polyethylenimine to act as an electron extraction layer on the polymer nanocomposite-based photovoltaic device [100]. The addition of the CDs to the interfacial layer led to a 12.2% increase of the photovoltaic performance when compared to the control devices. Furthermore, the power conversion efficiency was enhanced by 8.34% while the external quantum efficiency was enhanced by over 30% (around the 440 nm range) [100]. Other examples of CA-based CDs for photovoltaic devices can be found on [101, 102].

CDs: Heteroatom and Metal Doping

Over the course of the years, several strategies have been developed to enhance the photoluminescence intensity of CDs. The best-known example of this is that of modifying the nanoparticles' surface with heteroatoms in a process dubbed heteroatom doping. Doping is a useful process commonly used to increase the QY_{PL} of CDs. This is due to it prompting the formation of n- and p-type carriers (extra e^- and h^+), changing the CDs' electronic structure [103]. Thus far, heteroatom doping has been reported for elements such as nitrogen [68, 104], boron [12, 40], sulphur [96, 105] and phosphor [106, 107].

Among heteroatom doping, nitrogen-doped CDs are the most commonly used systems, as nitrogen atoms are known to affect the edge states, energy levels, catalytic activities and even physicochemical properties [108-110]. In

2021, Lee et al. published a study regarding the effect of N-doping on the optical properties and enzymatic activity of CDs [111]. Several CA and ethylenediamine-based CDs were prepared via a hydrothermal method, yielding CDs with a ratio of CA to ethylenediamine of 1:1.5 (N-CD1), 1:1 (N-CD2), 1:0.5 (N-CD3), 1:0.3 (N-CD4) and 1:0.25 (N-CD5). The CDs average sizes ranged between 5.9 and 13.7 nm, with the smallest particle being observed on N-CD3. FTIR analysis confirmed the presence of the same surface functional groups on all CDs (Table 1).

Table 1. Summary of data from high resolution analysis representing both band energies and corresponding groups

C *1s*	N *1s*	O *1s*
C-C / C=C – 284.0 eV	N-pyrrole – 399.5 eV	C=O – 531.1 eV
C-N – 288.5 eV	N-graphite – 401 eV (except N-CD1)	C-O = 532.6 eV
C=O – 288.2 eV		

The XPS profile of the CDs exhibits defined C_{1s}, N_{1s} and O_{1s} signals, as was expected. Interestingly, it also showed that N-CD2 displayed the highest N_{1s} peak, even though it was not made using the highest ratio of nitrogen-source. Further high-resolution analysis was performed. For C_{1s}, all CDs' display a peak at 284 eV ascribed C-C and C=C bonds (from carbon atoms in the carbogenic core of the nanoparticles), a peak at 285.5 eV attributed to C-N bonds (thus confirming the success of N-doping) and a peak at 288.2 eV derived from C=O bonds. Both C-N and C=O are peaks of carbon-heteroatom bonds, suggesting the presence of functional groups on the CDs' surface [111]. Furthermore, it was demonstrated that N-CD2, N-CD3 and N-CD4 present a high ratio of carbon-heteroatom bonds and that the N_{1s} spectra of all CDs shows a peak attributed to N-pyrrole (399.5 eV) at the edge sites of the carbogenic domain and a peak of N-graphite (401 eV) on the sp^2 carbon domain (except on N-CD1) [111].

Finally, the O_{1s} spectra shows two peaks at 532.6 and 531.1 eV, corresponding to C-O and C=O bonds, with the latter being predominant due to the polymerization of the material via amide bond formation [111]. This demonstrates that while the same dopant was employed on all synthesis, it led to different outcomes depending on the carbon:nitrogen ratio.

Lee's team then proceeded to investigate the optical properties of the N-doped CDs. First, they observed that a new absorption band at 340 nm (C=O, assigned to n-π* edge transition) and a shoulder at 240 nm (-C=C-, ascribed to π-π* on sp^2 carbogenic core) appeared when compared to non-doped CDs [111]. Secondly, each N-doped CD presented a different photoluminescence spectrum when excited at 350 nm. When excited, N-CD1 and N-CD2 emission presented two bands (450/517 nm and 450/500 nm, respectively), whereas N-CDs 3, 4 and 5 exhibited only one emission band (450, 450 and 464 nm, respectively) [111].

It is considered that graphitic domains may induce red-shifts on the particles emission, whereas pyrrolic domains do not affect the band gap of the carbogenic domains [112]. However, N-CDs 1,2 and 5 all show red-shifted emissions, despite containing mostly pyrrole functional groups. Given that a higher number of edge functional groups leads to a decrease in the size of p-conjugated carbogenic domains, it can be considered that N-CDs 3 and 4, which present a relatively low carbon content, emit lower-wavelength, higher-energy, radiation due to the small size of the p-conjugated carbogenic domains, which are, on the other hand, of expanded size in N-CDs 1,2 and 5 [111].

The QY_{PL} of the CDs was also measured. By order (N-CD1 to 5), the QY_{PL} were estimated to be 6.6, 15.1, 22.6, 14.9 and 9.3%, respectively, which is higher than the 3% calculated for non-doped CDs. The optimal carbon:nitrogen ratio for QY_{PL} was 1:0.5 (N-CD3), with lower N contents decreasing the $QY_{PL.}$ N-CDs 1 and 2 presented also lower QY_{PL} despite their higher N content, something that can be attributed to the generation of long-lived defect states on the nanoparticles' surface by the large quantities of N dopant [111, 113]. Finally, the photoluminescence lifetimes of N-doped CDs are longer than that of non-doped CDs due to the surface passivation of the CDs decreasing the non-radiative recombination and self-trapping of excitons [111]. All being said, the content of N-dopant included during the CDs synthesis is a crucial factor affecting their optical properties, which are of paramount importance for most CD-related applications.

Furthermore, Lee's team explored the use of the N-doped CDs as a nanozyme platform, which is a material that can catalyze enzymatic reaction and presents similar kinetics and mechanisms to those of naturally occurring enzymes [111]. Considering previous reports, the team decided to assess the peroxidase-like activity of the nanoparticles (Figure 5). This was achieved by monitoring the oxidation of 3,3',5,5'-tetramethylbenzidine (TMB) with hydrogen peroxide at pH2. By introducing N-doped CDs in the solution, the color changes from pale green to blue, an indicative of the oxidation of TMB. The amount of oxidized TMB, as quantified by the absorbance value at 652 nm, gradually increases due to the enzymatic reaction in the presence of both non-doped and N-doped CDs. However, N-doped CDs promoted a faster rate of TMB oxidation than non-doped CDs, which is shown by the higher initial velocity of the reaction presented by all the N-doped CDs when compared to the non-doped variant [111]. This may be a result of the high amount of C=O groups present in N-doped CDs, which are reported to act as catalytic sites [114]. Additionally, graphitic N atoms promote the adsorption of molecular oxygen to generate ROS. In conjugation, abundant C=O groups and graphitic N atoms promote a relatively high peroxidase-like activity [111].

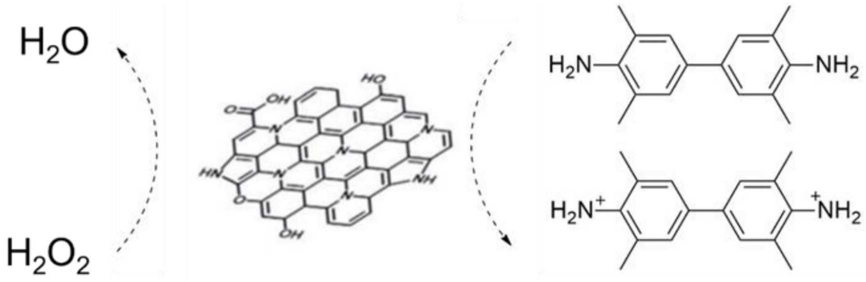

Figure 5. Schematic representation of the suggested peroxidase-like activity of N-doped CDs.

The number of possible heteroatom dopants and their combinations might result in a variety of properties which are not possible with undoped CDs. To study this, and considering the different types of heteroatom dopants and properties resulting thereof, Wibrianto et al. compared the effects of the synthesis of B, N, S or P-doped CA-based CDs, prepared by either furnace-assisted or microwave-assisted carbonization [115]. The CDs were fabricated by combining CA with either boric (B-CDs), nitric (N-CDs), sulfuric (S-CDs) or phosphoric acid (P-CDs), or no dopant at all (CDs).

In the furnace-assisted synthesis (x-CDs1, x = dopant), the mixtures were calcinated at 300 ºC for 2 h, whereas the microwave-assisted synthesis (x-CDs2) consisted of subjecting the mixtures to a microwave system with 600 W and high heat for 2 h. In either case, after the reaction the samples were dissolved in NaOH and the pH was set to neutral.

Finally, the solution was dialyzed using a dialysis bag with a MWCO of 1 kDa to exclude by-products and specify the CDs' size distribution [115]. After the synthesis, FTIR analysis confirmed the presence of common functional groups (O-H, C-H, C-O, C=O and C=C) in all the prepared CDs. However, specific dopant-derived groups are also to be found, such as B-O, S=C, C-N and P-O-C, confirming the success of the doping process by both pyrolysis and microwave-assisted synthesis [115].

It is commonly accepted that besides size confinement and solvent effects, the photoluminescence of CDs may result from a synergy between sp^2-conjugated atoms on the CDs' core with functional groups present on the nanoparticles' surface [116, 117]. As the use of different dopants inherently results in a different surface composition, it is expected to affect both the resulting CDs' band gap and the absorption-emission profile of the nanoparticle.

Optical analysis revealed that while maximum absorption and absorption peaks are quite similar using both furnace- and microwave-assisted methods, this is not true for the energy band gaps presented by the nanoparticles [115]. Band gap values between 4.52 and 5.37 eV were found for the CDs and their order (in terms of dopants) changes depending on whether the CDs were prepared via furnace- or microwave-assisted synthesis. The band gap sequence when using the furnace method is B-CDs1 < S-CDs1 < CDs1 < N-CDs1 < P-CDs1, whereas when using microwave irradiation we have P-CDs2 < S-CDs2 < CDs2 < N-CDs2 < B-CDs2. Both P-CDs and B-CDs presented both the lowest or the highest energy band gaps, depending on the method [115]. While the differences could be due to the difficulty of controlling the precise structure of the CDs, additional studies using another CD system suggest that the thermal induction from microwave irradiation can set carbonization. In this case, the position of doped atoms matches with the proposed structure. Using a microwave rather than the furnace allows a fast, efficient, heating of material through direct energy transfer, thus reducing the energy dissipation responsible for damage to the CDs' structure and allowing a more effective carbonization [118].

Moreover, the band gaps are also affected by the doping type of the used elements. Whereas B, N and P are mostly n-type dopants, S acts as a p-type dopant on CDs, which may result in a constriction of the original band gap [119]. When it comes to photoluminescence, all CDs demonstrated a strong blue emission (peaks between 410-445 nm) when excited at 360 nm [115]. Most CDs (except for B-CDs2 and N-CDs2) demonstrated an excitation-dependent photoluminescence, a common characteristic of CDs that happens due to the defect state caused by the oxygenated groups on CDs [38]. All CDs were similar in terms of photoluminescence quantum yields with a slight enhancement of the emission intensity being obtained through doping, with the values ranging between 31.17% (CDs2) and 32.96% (B-CDs2) [115].

Aside from heteroatom doping, CDs can also be doped using metals such as zinc [120, 121], manganese [122], copper [123, 124], gold [125] and silver [125], among others. Metallic ions can be used as electron donors in CDs, enhance the electron transfer capacity and ultimately confer new applications to the CDs. However, contrary to heteroatom-doped CDs, the majority of metal-doped CDs present a low QY_{PL} and an unclear mechanism for their photoluminescence.

Gencer et al. studied Zn(II)-incorporated CDs prepared from citric acid and zinc chloride via a microwave-assisted synthesis [121]. Two different molar ratios of CA:Zn were chosen, 1:1 (Zn(1)-CDs) and 1:10 (Zn(10)-CDs). After synthesis, the authors characterized the CDs. Differences were also observed using FTIR. In Zn(1)-CDs and Zn(10)-Cds, peaks attributed to C-O and C=O stretching partially of fully disappear, giving place to a new peak corresponding to the asymmetric stretching of COO^- groups present in zinc carboxylate [121]. These results imply that carboxylic groups on the CDs' surface are passivated as Zn(II) is added. A complete XPS survey also confirmed the presence of Zn in the CDs. Importantly, as the Zn quantity is increased, a peak attributed to CO^- gradually decreases as Zn passivate these groups, increasing the stability of the CDs.

Regarding photoluminescence, the team found that Zn(1)-CDs' photoluminescence was largely diminished when using a 1:1 ratio of CA:Zn. However, the emission intensity increased considerably in the Zn(10)-CDs compared to the non-doped CDs, with the CDs presenting QY_{PL} of 20 and 51%, respectively [121]. Furthermore, Zn(10)-CDs presented a narrower, red-shifted emission peak when compared to normal CDs, suggesting that incorporating Zn(II) in the CDs leads to an increase of non-radiative transitions, possibly due to causing heterogeneity in the CDs' structure. Whereas this would normally result in a decreased QY_{PL}, as the amount of zinc is increased the CDs' structure start to become homogeneous, resulting in a QY_{PL} higher than that of the normal CDs [121].

The photoluminescence excitation spectrum of the CDs also changed upon incorporation of Zn(II). Whereas the CDs presented two excitation peaks (288 and 343 nm) before the addition of Zn, Zn(1)-CDs nor presents three excitation peaks at 264, 325 and 400 nm (λ_{em} = 440 nm). When the Zn ratio was further increased and Zn(10)-CDs again presented 2 different peaks (281 and 372 nm), presenting an excitation spectrum closer to that of the conventional CDs, albeit with slightly different peak positions. These changes in the excitation and emission profiles of the CDs indicate that adding Zn(II) first results in defects in the CDs' structure (increasing heterogeneity), but later starts contributing to the homogeneity of the nanoparticles as the Zn amount increases [121]. This explains the decrease and then increase in QY_{PL} of the CDs as Zn is added and also the similarity between the excitation spectra of CDs and Zn(10)-CDs and the difference between those and that of Zn(1)-CDs.

Finally, a nearly excitation-independent emission occurs in Zn(10)-CDs, which may derive from the high degree of passivation of the CDs' surface with Zn(II) [121]. The summary of these results illustrates the major differences that one can obtain when doping CDs with a metal dopant in terms of photophysical properties and how it can be used to tailor CDs to specific applications.

CDs: Impurities and Respective Consequences

Although the number of studies concerning CDs has been growing year after years, the origin of their main point of interest, their photoluminescence, is still a matter of debate. Thus far several models and possible explanations have been presented by the scientific study, including the quantum confinement effect and band gap emission [126], surface states emission [127], self-trapped excitons [128], surface dipole emissive centers [129], H-type aggregates excitonic states formation [130], among others. More recently, the role of molecular fluorophores formed during the CD synthesis on the nanoparticles' photoluminescence has also been under focus.

It has been previously reported in several studies that during the bottom-up synthesis of CDs, which is arguably the majority of the cases, leads to the production of several molecular by-products alongside the CDs during their synthesis [49, 131, 132]. This is of considerable importance when we take into account that these by-products possess an intense fluorescence that is significantly higher than that of the nanoparticles themselves. Thus, unless the synthesis products are thoroughly purified via methods such as dialysis or chromatography, the fluorescence associated to a CD solution could result instead of these molecular by-products, constituting a significant setback of our knowledge database regarding theses nanomaterials.

To study this, Sendão et al. studied the photoluminescence displayed by CDs and the molecular by-products resulting of their synthesis, as well as how these molecular fluorophores might affect the CDs' photochemical properties and reactivity [22]. To this end, CA and urea-based CDs were synthesized via a microwave-assisted methodology and purified via centrifugation and dialysis, yielding different fractions (Figure 6): $CD_{centrifuged}$, containing both the CDs and the molecular by-products (which are low-weight and soluble) and obtained after a simple centrifugation to remove insoluble particles after the synthesis; $CD_{dialyzed}$, containing only the CD and obtained by dialyzing the synthesis products over 72 h with a MWCO of 1 kDa; and $Water_{FI}$, containing the smaller molecular by-products (whose relatively small size compared to CDs allows them to cross the dialysis bad membrane while CDs are retained) and obtained by collecting the dialysis wash water resulting from the CDs' dialysis [22, 131].

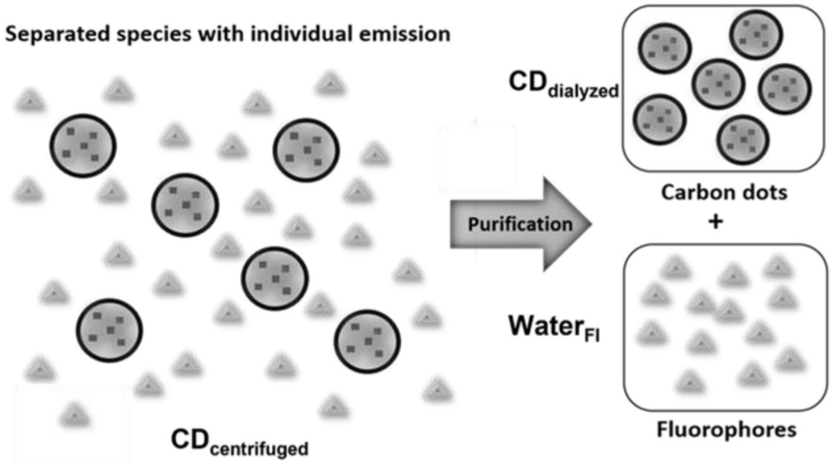

Figure 6. Schematic representation of the different fractions obtained before and after dialysis of an unpurified CDs solution.

The authors started by analyzing the CDs' structure both with and without the presence of the by-products. A full XPS survey followed by detailed scans for the C_{1s}, O_{1s} and N_{1s} levels was made. Both in the presence and absence of the by-products ($CD_{centrifuged}$ and $CD_{dialyzed}$, respectively) the CDs' fractions results are quite similar, except for a very slight increase of the C content and subsequent decrease of N and O content. Thus, the CDs' surface composition is identical between the fractions and dialysis has a limited effect on the nanoparticles [22]. This is further supported by FTIR analysis, which revealed similar spectra for both fractions.

However, this similarity is not corroborated by optical analysis. The UV-Vis absorption spectrum (Figure 7a) of $\text{CD}_{\text{dialyzed}}$ displays a band at 340 nm and a shoulder at 245 nm, which can be ascribed to n-π and π-π* transitions (C=C and C-N bonds), respectively, and an additional less discernible small band at 410 nm [22]. By its turn, the $\text{CD}_{\text{centrifuged}}$ sample presents two shoulders (245 and 275 nm), and a well-resolved band at 410 nm that is now higher than the one at 340 nm. Furthermore, the two CD-containing fractions present a major difference in terms of photoluminescence (Figure 7b), despite both presenting an excitation-dependent emission. Whereas the $\text{CD}_{\text{centrifuged}}$ samples presents an emission peak at 550 nm, the $\text{CD}_{\text{dialyzed}}$ peak is considerably blue-shifted to 475 nm.

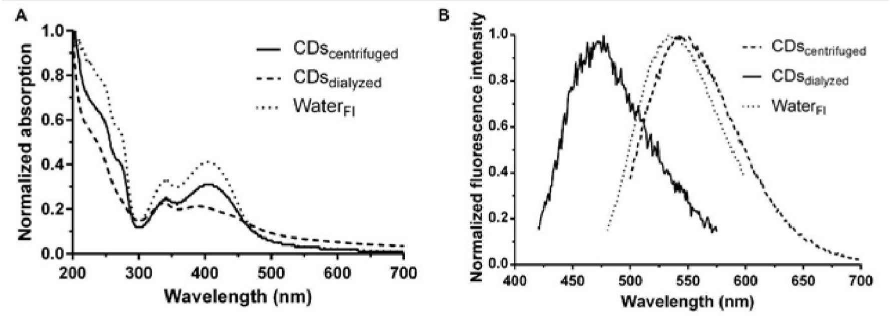

Figure 7. a) Normalized UV-Vis absorption spectra, and b) Normalized emission spectra for $\text{CD}_{\text{centrifuged}}$ (λ_{exc} = 410 nm), $\text{CD}_{\text{dialyzed}}$ (λ_{exc} = 380 nm) and Water_{FI} (λ_{exc} = 410 nm). Reproduced with authorization from [22].

Additionally, the excitation wavelength maxima also change from 410 nm to 380 nm after the dialysis. Thus, purification by dialysis significantly affects the photoluminescence of the CDs and the differences between the optical properties of two fractions can be ascribed to the presence (or absence) of the molecular by-products. This is further confirmed by the fact that the Water_{FI} fraction, containing only the synthesis by-products, reveals an emission profile almost identical to that of $\text{CD}_{\text{centrifuged}}$. Specifically, Water_{FI} maximum excitation and emission wavelengths are 410 and 540 nm, respectively, and its absorption spectrum displays the same bands and shoulders as $\text{CD}_{\text{centrifuged}}$.

Furthermore, the $\text{CD}_{\text{centrifuged}}$ and Water_{FI} samples present emission intensities of the same magnitude that are 6-8 times higher than those of $\text{CD}_{\text{dialyzed}}$ samples (the CDs by themselves). In summary, the optical properties observed on the $\text{CD}_{\text{centrifuged}}$ sample are not a result of the CDs themselves, but rather a result of the properties of the low-weight highly fluorescent by-products which mask the emission of the carbon nanoparticles [22].

Knowing this, the authors employed mass spectroscopic analysis via ESI-MS to evaluate the samples. While not being enough to fully determine the molecular species behind the $CD_{centrifuged}$ fluorescence, it confirmed that the bottom-up synthesis of CDs results in a mixture of CDs and fluorescent by-products that require further purification steps to separate the fractions [22, 131]. Nevertheless, despite not being able to positively identify the by-products, the authors point that in the ESI-MS analysis a predominant peak, common both to $CD_{centrifuged}$ and $Water_{FI}$, but absent in the $CD_{dialyzed}$ fraction, is identified and can be attributed to 4-hydroxy-1H-pyrrolo[3,4-c]pyridine 1,3,6(2H,5H)-trione (HPPT, M.W. of 180 g mol^{-1}) [22].

HPPT was already reported by Kasprzyk et al. as being a photoluminescence by-product that resulted from the microwave-assisted synthesis of CDs [132]. Furthermore, HPPT is known to have a green emission with an absorption peak at 410, which is quite in line with the properties of both $CD_{centrifuged}$ and $Water_{FI}$. Thus, HPPT seems to be the main responsible for the CDs' photoluminescence in the $CD_{centrifuged}$ sample but, as it is removed during dialysis, it is no longer present in the $CD_{dialyzed}$ samples, explaining the difference in the properties [22].

Besides affecting the optical properties of the CDs, the presence of molecular by-products also affected the way in which the nanoparticles responded to other parameters [22]. By measuring the fractions' photoluminescence in water, HCl (0.1 M) and NaOH (0.1 M), the team confirmed that the impurities conferred pH sensitivity. Both $CD_{centrifuged}$ and $Water_{FI}$ suffered a blue-shift at basic pH while $CD_{dialyzed}$ presents no change whatsoever with the different pH. A similar study was performed by analyzing the photoluminescence spectra of the fractions in different solves, namely methanol (MeOH), acetonitrile (CAN), dimethylformamide (DMF) and dimethyl sulfoxide (DMSO).

Again, despite the range of properties of the different solvents, they had a negligible effect on $CD_{dialyzed}$, possible suggesting that the emissive moieties of the CDs are inside the nanoparticle, and so, not exposed to surrounding microenvironment [133]. By its turn, the emission spectra of $Water_{FI}$ suffers a blue-shift when compared to the 540 nm peak in water. This indicates that the fluorescent moieties are exposed to the external medium, and thus affected by it.

Interestingly, $CD_{centrifuged}$ shows an intermediate effect, in which there is also a blue-shift, but of a lesser extent of that of $Water_{FI}$. This would indicate that like in Water_{FI} the fluorescent moieties are exposed to the solvent, however, they are also somewhat more shielded of the solvents effect. Thus, in the same way that the CDs' photoluminescence is affected by the by-products, the CDs' by their turn also affect the fluorescent properties of the molecular by-products [22].

Alongside altering the optical properties of CDs, the molecular by-products of their bottom-up synthesis also seem to alter the excited state reactivity of the nanoparticles. The photoluminescent response of the three fractions was analyzed in the presence of both electron-donor and electron-acceptor molecules, diphenylamine (DPA) and nitromethane (NM), respectively [22]. The comparison of the responses of the individual parts ($\text{CD}_{\text{dialyzed}}$ and Water_{FI}, Figures 8b and 8c, respectively) with that of the whole ($\text{CD}_{\text{centrifuged}}$, Figure 8a) permitted to verify the existence of a synergistic effect which was more than just the sum of the effects of the individual parts.

Starting with the fractions' response to the electron-donating molecule, DPA, it was observed that the three different fractions presented a different response to increasingly higher concentrations of DPA. The photoluminescence of $\text{CD}_{\text{centrifuged}}$ was quenched ($K_{SV} = 0.0054\ \mu M^{-1}$), whereas in $\text{CD}_{\text{dialyzed}}$ the opposite effect was observed, with the fluorescence intensity increasing with rising concentrations of DPA. Interestingly, DPA seemed to have no effect whatsoever on Water_{FI}. These results suggest that the DPA-induced quenching observed on $\text{CD}_{\text{centrifuged}}$ could not be a result neither from the CDs themselves nor the by-products resulting of their synthesis, both of which presented different responses to DPA than $\text{CD}_{\text{centrifuged}}$. Thus, we are left with the conclusion that, when combined in solution, the CDs and the by-products may interact and generate a synergistic effect resulting in a different response to DPA than that of either individual species [22].

When evaluating the fractions response to the electron-withdrawing molecule, it was observed that NM induced quenching in all samples (Figure 8d), suggesting that all fractions are capable of PET reactions by acting as an electron-donor. However, when irradiated at their maximum excitation, the photoluminescence $\text{CD}_{\text{dialyzed}}$ is considerably more quenched (Stern-Volmer constant, $K_{SV} = 23.7 \pm 0.1\ \mu M^{-1}$) than $\text{CD}_{\text{centrifuged}}$ and Water_{FI} ($K_{SV} = 5.4 \pm 0.2\ \mu M^{-1}$ and $K_{SV} = 6.1 \pm 0.4\ \mu M^{-1}$, respectively), which present a similar response to NM.

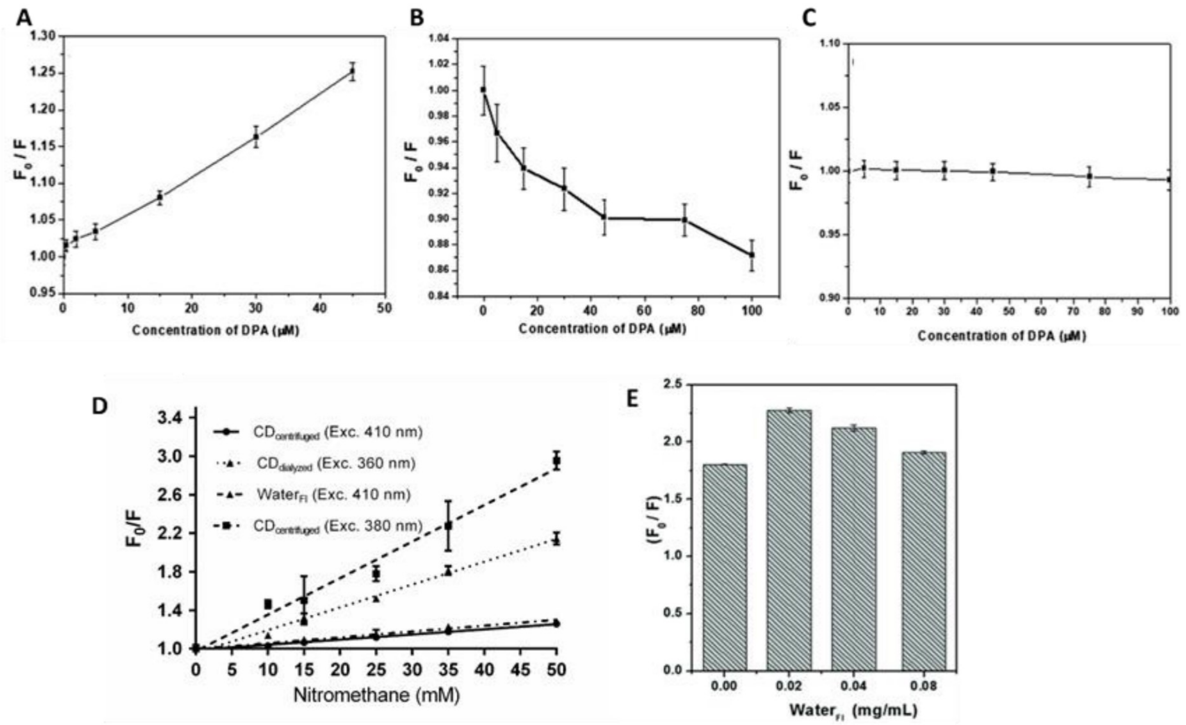

Figure 8. F_0/F correlation for A) $CD_{centrifuged}$, B) $CD_{dialyzed}$ and C) $Water_{FI}$ with increasing concentrations of DPA. D) F_0/F correlation for all fractions with increasing concentrations of NM. E) Variation of F_0/F of a constant amount of $CD_{dialyzed}$ and NM, but varying concentrations of $Water_{FI}$. In all cases, positive F_0/F values indicate quenching, whereas a negative value indicates an enhancement of the photoluminescence. F_0 – Photoluminescence intensity in the absence of DPA or NM; F – photoluminescence intensity with a given amount of DPA or NM. Reproduced with authorization from [22].

Furthermore, considering the synergistic effect previously observed with DPA, the team analyzed $CD_{centrifuged}$ response to NM, but changed the excitation wavelength to that used for $CD_{dialyzed}$. This yielded interesting results, as using a 380 nm excitation resulted in a new shoulder in the emission spectrum (at around 460 nm), which can be attributed to the emission of the nanoparticle itself, as it lines neatly with the emission peak observed with $CD_{dialyzed}$. Monitoring the new peak allowed the team to evaluate the response of the CDs themselves, but still in the presence of the fluorescent by-products. In this case, the photoluminescence of the CDs again presented quenching in the presence of NM, but in a much larger scale than before ($K_{SV} = 38.0 \pm 2.5$ μM^{-1} *versus* 23.7 ± 0.1 μM^{-1} obtained for $CD_{dialyzed}$). The presence of the by-products enhanced the NM-induced quenching of the nanoparticles themselves, and, considering that $Water_{FI}$ do not suffer significant quenching by themselves ($K_{SV} = 6.1 \pm 0.4$ μM^{-1}), the larger extent of the quenching must be a result of the synergistic effect previously observed between the CDs and the fluorescent by-products [22].

Finally, to confirm if the by-products can in fact modulate the photochemical reactivity of the nanoparticles, the photoluminescent response of a constant amount of $CD_{dialyzed}$ towards NM was evaluated in the presence increasing concentrations of $Water_{FI}$ (Figure 8e). The addition of the by-products did indeed increase the NM-derived quenching at the start. However, this effect decreases as the amounts of $Water_{FI}$ added increase. The proposed reason for this is that the by-products interact with the CDs and prompt the formation of a hybrid material presenting synergistic properties. However, increasing the amount of by-products added beyond a certain threshold may mask the surface of the CDs, preventing its interaction with the quencher and thus limiting the effect observed resulting from the synergy [22].

In summary, the work of Sendão et al. provides an example of why the by-products that may result from a CD bottom-up synthesis must be taken into consideration [22]. They successfully demonstrated that these by-products may mask the photoluminescence of the CDs and, more importantly, they may react with the CDs in solution and give rise to a synergistic effect that may affect not only the optoelectronic properties of the nanoparticles, but also their photochemical reactivity to other compounds, such as DPA and NM [22]. If required, these by-products may be removed from the CDs' solution via purification through dialysis or chromatography. However, the potential of discovering new applications based on the hybrid photoluminescence and reactivity resulting from the synergistic effect between CDs and molecular by-products may justify a deeper study of these hybrid materials.

Environmental Impact of CA and Natural Alternatives to Its Use

The last part of this chapter concerns itself with the sustainability of CA-based CDs. It is known that engineered nanomaterials have different properties than their respective bulk materials, and this led to an increased exploration of their potential. However, the environmental impacts resulting from their synthesis and use is still quite unclear [134]. This led to studies aiming to understand the impact of the nanomaterials during their life cycle. Studies based on a life cycle assessment (LCA) of the products were employed, as it permitted to quantify the environmental impacts of system during its life cycle based on information inventories [135, 136].

Regarding CDs, studies regarding the potential environmental impacts of different synthetic conditions are available [31, 34, 137]. This is of particular importance, as the production stage of engineered nanomaterials was already identified of consisting of an important environmental concern, as it can be orders of magnitude more material and energy-consuming than pharmaceuticals and fine chemicals [138]. In particular, the electricity and chemicals used during the synthesis are major contributors to the resulting environmental impact of a product during its life cycle [131].

One of the first studies considering the environmental impacts resulting from the synthesis of CDs was the work of Sendão et al. who, via LCA, compared the relative environmental impacts of bottom-up synthetic routes for the production of CA,urea-based CDs [31]. Six representative bottom-up strategies were analyzed via a cradle-to-gate LCA. The routes consisted of the hydrothermal of microwave-assisted synthesis of CA or CA,urea-based CDs. The results were presented regarding the three endpoint categories of environmental impacts (human health, ecosystems and resources). In general, hydrothermal treatments presents more environmental impacts than microwave-assisted synthesis due to the high energy usage. However, whereas electricity is the main contributor towards the impact of hydrothermal synthetic routes, the carbon source (in this case CA) is the major responsible behind the impacts associated to microwave-assisted synthesis, meaning that it is also an important factor for the environmental impact of the resulting particles [31].

Finally, a sensitivity analysis based on the change of the carbon precursors conditions was performed. In hydrothermal-based procedures, changing the amount of carbon precursor by ±30% leads only to a moderate effect (impact variation of around 6%), whereas changing the carbon precursors from CA to glucose led to a 15% decrease of the impact in all three main categories. By its turn, in microwave-assisted synthesis, varying the amount of CA caused a more significant variation of the environmental impacts (between 10 and 16%), in part due to the low contribution of electricity in this strategy. Furthermore, replacing CA with glucose led to a drastic decrease in the environmental impacts in all categories: 44% in human health, 33% in ecosystems and 27% in categories, further confirming the influence of the carbon precursor in the sustainability of a synthetic strategy [31].

Another study, by Christé et al., studied the environmental impact of different N-doping strategies in the synthesis of the nanoparticles [34]. N-doped CDs were prepared via a bottom-up strategy from CA with either small organic molecules (urea and ethylenediamine) or N-containing organic solves (such as *N*,*N*-dimethylformamide, acetonitrile and pyridine). For CA,urea- and CA,ethylenediamine-based CDs, the highest contributor towards environmental impacts was the carbon source (CA) in almost every category [34]. The contribution of electricity was small due to the small irradiation times inherent to microwave-assisted synthesis. Regarding the CDs prepared with CA and N-containing solvents, generally, the main source of impact was from the solvents themselves. However, the carbon source is still the main factor of impact for categories such as land use and water consumption, being still a factor that needs to be accounted for [34].

Also using LCA, Fernandes et al. compared different high-yield synthetic routes for the production of CDs [137]. The routes included the production of hydrochar via hydrothermal treatment of carbon precursors and alkaline-peroxide treatment, and the thermal treatment of carbon sources mixed in a eutectic mixture of salts. In accordance with previous studies [31], Fernandes et al. found that the most crucial parameter affecting the environmental impacts is the identity of the carbon precursors, of which glucose yielded the lower impact when compared to CA and *para*-phenylenediamine [137].

Taking into consideration the abovementioned works [31, 34, 137], the role of the carbon precursor must be seriously considered when attempting the sustainable synthesis of CDs. Whereas the carbon precursor quantity might be of relative relevance, in particular when concerning less energy-intensive synthesis, the identity of the carbon precursor is always of major importance and must be considered. Even between commonly used commercial grade chemical reagents, such as CA and glucose, differences in terms of environmental impacts are observed. Choosing a more sustainable, if possible renewable, carbon precursor is an important step towards achieving environmental sustainability in the process. The alternative is the use of biomass, and some reports have already been published regarding the valorization of a waste or renewable material into the making of CDs [33, 47, 59, 139-143], thus promoting reusability, sustainability and a circular economy.

Crista et al. investigated the use of spent coffee grounds as a precursor for the sustainable making of CDs and compared them to CA and urea-based CDs in terms of environmental sustainability [141]. The use of spent coffee grounds takes advantage of the significant increase in the worldwide consumption of coffee seen in the past few years. As spent coffee grounds are known to possess organic compounds, such as carbohydrates, lipids and proteins, they are a good candidate for valorization and to be used in the making of CDs [144]. The CDs, obtained via a one-pot solvent-free carbonization of solid coffee grounds samples, generated CDs sized between 2.1 and 3.9 nm presenting an excitation-dependent blue photoluminescence and moderate QY_{PL} (2.9 – 5.8%), which are typical characteristics of CDs.

Furthermore, the CDs proved to be usable as photoluminescent probes for Fe(III) in water with a limit of detection as low as 3.51 µM (*versus* 3.07 µM for CA,urea-based CDs), confirming their potential applicability for sensing [141]. Finally, when the team analyzed the environmental impacts associated to the CDs via a LCA using a QY_{PL}-based functional unit they found that the coffee grounds-based CDs had a considerably lower environmental impact than the traditional CA,urea-based CDs in all categories. Thus, despite a lower synthesis yield and QY_{PL}, the coffee-based CDs are still an environmentally better option than the typical CA and urea precursors, even when considering a function based QY_{PL} functional unit [141].

Another example on the valorization of biomass is the work of Aggarwal et al., who prepared cellulose-based CDs for the photocatalytic removal of toxic Cr(VI) [59]. The cellulose was transformed into CDs via an acid-assisted one-step thermal carbonization (90ºC for 30 minutes). Within 120 minutes of sunlight irradiation the CDs were able to completely remove Cr(VI) ions (20 ppm) from wastewater. Thus, cellulose, a low cost, green, alternative carbon source, was used to prepare photoactive CDs for photocatalysis, making the overall process sustainable and economical [59].

Campalani et al. prepared CDs from fish scales, a carbon and nitrogen-rich waste material consisting mostly of chitin and collagen [33]. The hydrothermally prepared CDs were compared to CA and diethylenetriamine-based CDs, presenting a similar morphology and a higher initial methyl viologen photoreduction rate than the conventional alternative (despite presenting lower QY_{PL} and excited state lifetime) [33]. Wang and Zhou reported the synthesis of milk-based CDs for imaging applications [47]. The hydrothermal treatment of milk yielded highly photoluminescent CDs that were used for high resolution imaging of human brain glioma cells. The synthesis was simple and environmentally friendly, originating CDs from a widely available renewable source [47].

Thakur et al. reported the making of CDs from Citrus limetta waste pulp via a one-step pyrolysis procedure [143]. The CDs exhibited a high QY_{PL} (63.3%), which is above most conventional CDs. When tested, the CDs revealed potential for several applications, such as hydrogen production via water splitting, photocatalytic degradation of organic dyes, Fe(III) sensing, bactericidal activity versus *E. coli* and *S. aureus* and bioimaging [143]. The immense versatility of the CDs is an indicator of the wealth of potential of CDs prepared from waste products such as this. Furthermore, these CDs have the edge on both environmental sustainability and economy, as they use an otherwise useless biological waste to generate valuable products, promoting a circular economy.

Here, we are also to report the synthesis of new CDs by using an otherwise waste product to replace CA as the chosen carbon precursor. Namely, we are going to use corn stover as an alternative carbon source. Corn stover consists of the leaves, stalk and cobs of corn plant left on the field after harvest. It constitutes a significant agricultural waste that makes about half of the corn crop's yield [145]. Despite this, ninety percent of corn stover is discarded instead of being used for other applications [145]. Given this, corn stover appears as a waste material with potential for valorization as a carbon source for CDs. To dope CDs with heteroatoms, thiosulfate was introduced as an S-dopant.

Corn stover was collected from an agricultural area in Vairão, Portugal. The collected corn stover was first washed with deionized area and left to dry at 50ºC. Subsequently, the corn stover was shredded by employing a LAARMANN Power Cutting Mill CM 500, with a sieve of 0.5 mm. The resulting material was collected and stored at -80ºC. The CDs were then synthesized via thermal heating. Briefly, 0.25 g of processed corn stover and 0.25 g of sodium thiosulphate pentahydrate were weighted and mixed before being transferred into a *Teflon*-lined reactor with steel outer plating. The reactor was then transferred to an oven (VWR DL 112 Prime oven (2500 W power consumption) and subjected to a temperature of 225ºC for 4 hours. The resulting product was suspended in 10 mL of deionized water, which was followed by centrifugation (10000 rpm for 10 minutes) and dialysis (24 hours, MWCO of 1 kDa), after which a solution of purified CDs was obtained.

The particle size presented by individual CDs was estimated to be 1.28 ± 0.50 nm, as calculated from data obtained from AFM measurements (collected from 80 individual measurements). While individual CDs can be discerned and present a spherical shape, there can be observed some agglomerates in the AFM image (Figure 9). This can be attributed to the known tendency of CDs to aggregate [146, 147].

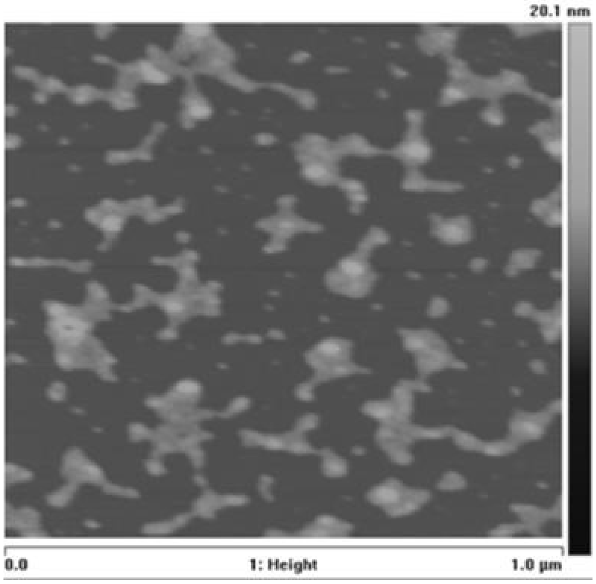

Figure 9. AFM image of the CD in a silica plate support. AFM was carried out using a Veeco Metrology Multimode/Nanoscope IVA by tapping. A silica plate was used to deposit the sample for analysis and an AFM TESP-SS cantilever (curvature radius of 2 nm) was used. The software used for the AFM data analysis was NanoScope.

The absorption spectrum of the CD displays a broad absorption ranging from the UV region and extending into the visible region. The spectrum is typical for the absorption displayed by CDs [22, 148, 149]. Furthermore, when the absorption and excitation spectra (obtained for the maximum emission wavelength of 470 nm) are overlapped (Figure 10) it is possible to observe that the maximum excitation wavelength (370 nm) falls outside the region in which the CDs absorb the most radiation.

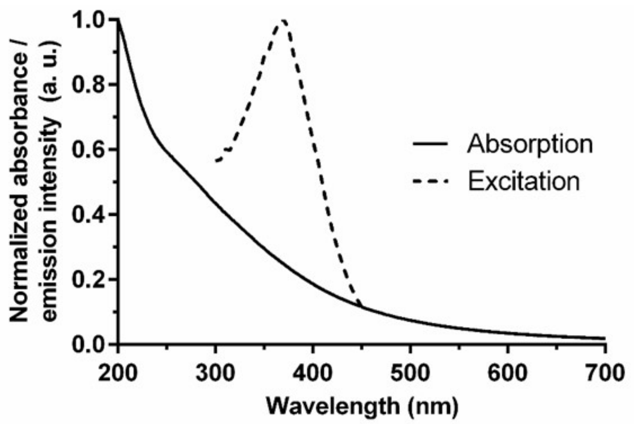

Figure 10. Absorption and excitation spectra of the CD in water. The absorption profile was recorded using a VWR® UV3100PC spectrophotometer. The excitation spectrum was obtained using a Horiba Jovin Yvon Fluoromax-4 spectrofluorimeter.

Regarding its photoluminescence (Figure 11a), the CD is capable of emitting light with an emission wavelength maximum of 470 nm, when excited both at 270 and 370 nm (two excitation maxima). Furthermore, it displays an excitation-dependent emission (Figure 11b), with the emission wavelength ranging between 470 and 550 nm for excitation wavelengths between 300 and 500 nm.

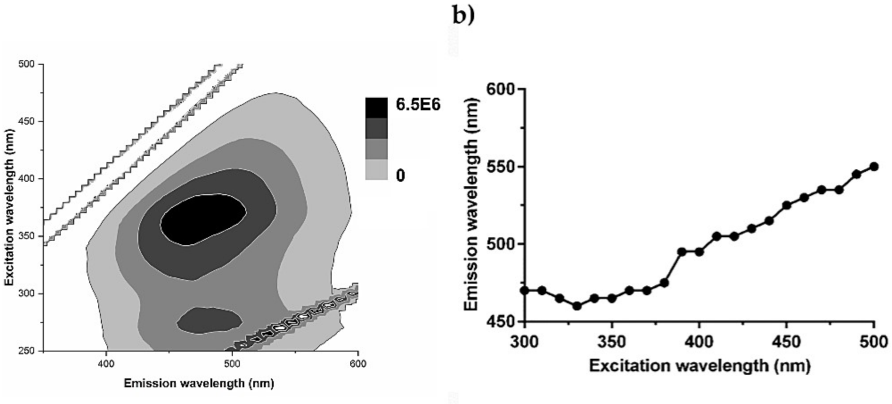

Figure 11. a) 2D excitation-emission matrix, EEM, contour surface;
b) Emission wavelength variation in function of the excitation wavelength. The photoluminescence profile of the CDs was analyzed, in aqueous solution, using a Horiba Jovin Yvon Fluoromax-4 spectrofluorimeter. Standard fluorescence quartz cells were used.

To better understand the surface composition and electronic states of the elements present in the CDs, an XPS analysis was performed. It revealed that the surface of the CDs is composed mainly of C, O, N and S, with a content (in %) of 65.6, 20.9, 1.3 and 4.1%, respectively. These elements are to be expected from the composition of corn stover and sodium thiosulfate [150], which were used as precursors for these CDs.

A scan for the C_{1s}, O_{1s}, N_{1s} and S_{2p} internal levels for deconvolution and chemical state was subsequently performed (Figure 12). Regarding the C_{1s} core level spectrum, after deconvolution it splits into five peaks. Binding energies of 285.0 eV (70.32%), 286.4 eV (16.22%), 287.0 eV (3.99%), 288.3 eV (7.81%) and 289.5 eV (1.66%) were detected. The observed C_{1s} peaks are attributed to C-C/C-H/adventitious carbon (285.0 eV), C-N/C-S/C-O (286.4-287.0 eV), C=O/O-C=O carbonyl/carboxylic groups (288.3 eV) and C-O-C ether groups (289.5 eV). Regarding the O_{1s} core level spectrum, when deconvoluted, a major peak at 531.9 eV (92.38%) and a smaller one at 539.3 eV (7.62%), ascribed to carbonyl (C=O) linkage and C-O/O-C-O groups, respectively. By its turn, the deconvolution of the N_{1s} core level spectrum yielded a major peak at 400.0 eV (96.09%) and a shoulder at around 401.8 eV (3.91%), attributed to groups of amines/amides and protonated amines, respectively. Finally, the deconvolution of the S_{2p} core level spectrum results in two similar peaks at 164.5 eV (50.22%) and 168.9 eV (49.78%).

Having characterized the obtained CDs, we have then investigated the potential effect of these CDs on a marine chemiluminescent reaction. Chemiluminescence consists in the emission of light due to a chemical reaction, with a sub-type of chemiluminescence being bioluminescence, in which light is emitted due to a biochemical reaction. Both chemi- and bioluminescent reactions present a diminished probability for autofluorescence arising from the background signal, thereby increasing the signal-to-noise ratio. So, these systems can generate luminescent signals with high sensitivity and almost no background noise. This is a very important feature, which explains why chemi- and bioluminescence have been gaining practical applications in fields such as sensing and bioimaging [151-153]. One of the most well-known chemi- and bioluminescent systems is that of Coelenterazine, a substrate widely found in marine species [154, 155]. More specifically, it is capable of both bioluminescence (in the presence of either photoproteins or luciferase enzymes) or chemiluminescence (in polar aprotic solvents, such as DMF or DMSO) [156, 157].

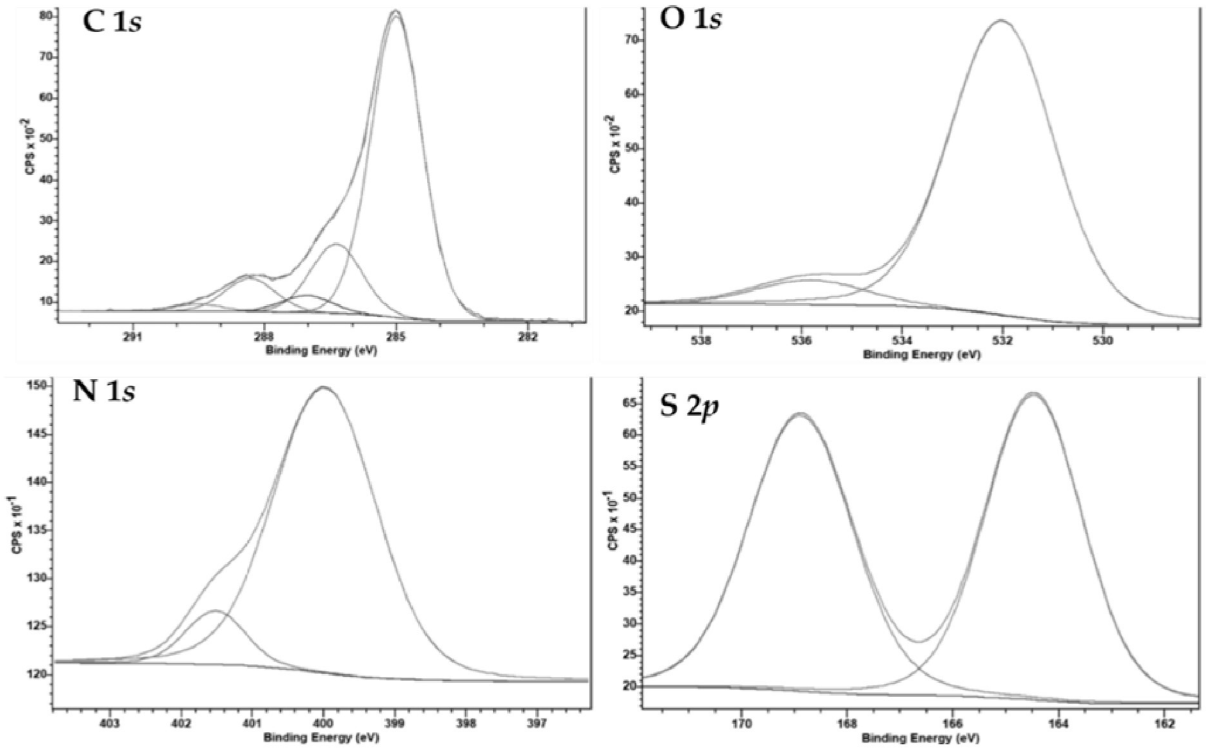

Figure 12. XPS core level spectra of the CD: a) C 1s b) O 1s, c) N 1s and d) S 2p. X-Ray Photoelectron Spectroscopy (XPS) was carried out using a Kratos Axis Ultra HSA spectrometer utilizing Al monochromatic radiation with a hemispherical multichannel detector (90 W and 15 kV). The was deposited upon a silicon wafer. CasaXPS software was used to analyze the results and the carbon C 1s signal, 285.0 eV, was used as a reference to obtain the binding energy values, using Gauss-Lorentz curves and Shirley-type background.

The energy necessary to promote a chemical species to an electronically excited state can be obtained from a chemical reaction involving high-energy intermediates. This type of process is essential for chemi- and bioluminescence, and involves high-energy peroxide intermediates, such as dioxetanes and dioxetanones [158, 159]. In the case of Coelenterazine, the high-energy intermediate is a dioxetanone-based compound [160]. It should be noted that despite decades of research, the mechanism behind efficient chemiexcitation is still not fully understood.

The Chemically Induced Electron-Exchange Luminescence (CIEEL) was the first to be employed in attempts to rationalize these processes and consists in electron transfer from an electron-rich group to the peroxide, followed by back electron transfer. This latter step leads to chemiexcitation due to charge annihilation [161]. Interestingly, within this context, it was found that oxidizable fluorophores can activate the decomposition of some high-energy peroxide intermediates, leading to ground state carbonyl compounds and to the excitation to the fluorophore in its first singlet excited state [159].

To our knowledge, there is no information regarding either if CDs can be used as fluorophores and activators, or if the chemiluminescence of Coelenterazine could be catalyzed in such a way. Thus, we have tested the CDs referred to above, produced from corn stover and sodium thiosulfate, as possible activator/catalyst for the chemiluminescent reaction of marine Coelenterazine.

The chemiluminescent kinetic curves, in the presence or absence of the CDs, can be found on Figure 13. Qualitatively, the resulting kinetic profiles are quite similar. However, and more interestingly, the chemiluminescence reaction, which occurred in the presence of CDs, showed an increase of the light-emission maxima when comparing with the reaction that occurred in the absence of the CDs (1.24 ± 0.14). When reducing the concentrations of both Coelenterazine and CDs to half, but maintaining the same relationship between them, the results are similar (1.36 ± 0.16). Thus, the CDs showed an ability to enhance, at least moderately, the chemiluminescence emission of Coelenterazine.

To our knowledge, this is the first report of CDs being able to enhance the light-emission of a chemiluminescent reaction, with focus on the coelenterazine system.

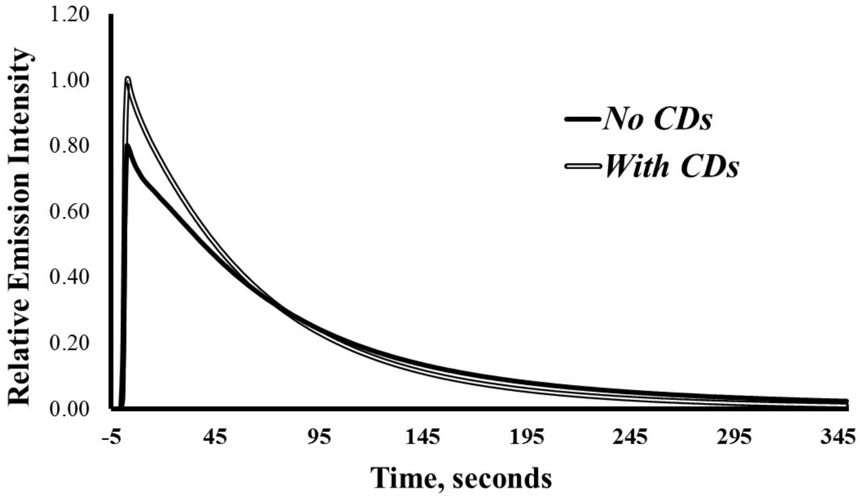

Figure 13. Relative emission intensity, as a function of time, of the chemiluminescent reaction of marine Coelenterazine in DMSO, in the presence and absence of CDs. The chemiluminescence kinetics were measured in a homemade luminometer, in which a Hamamatsu HC135-01 photomultiplier tube is found. The light was integrated and recorded in 1 second intervals. Measurements were performed in DMSO with a final volume of 500 µL. The concentration of Coelenterazine was of eight µM and the CDs of 0.002 g/l. Assays were made at least in quintuplicate.

Having made this discovery, the next step was to try to find if this enhancement was due to a CIEEL-like mechanism, in which the CDs act as activators and as the light-emitters. To that end, we have measured the chemiluminescent spectra of Coelenterazine reaction, in DMSO and in both the presence and absence of CDs (Figure 14).

Quite interestingly, there is an essentially total overlap between the spectra obtained in the presence and absence of CDs, which indicates that there is no contribution to light-emission from the CDs directly. In fact, the obtained chemiluminescent spectra are consistent with that of just Coelenterazine [154]. More importantly, the fluorescence quantum yield of the CDs was determined by using quinine sulfate [31, 141, 162]. The obtained value was quite low, and of just ~0.7% (also meaning that there is the need for further optimization of synthesis reactions involving corn stover as a precursor, if the aim is the production of highly luminescent CDs). Thus, if the chemiluminescent reaction led to the excitation of CDs, we would probably see a relevant decrease in light-emission, and not an increase. So, these results indicate that the CDs are acting as catalysts of the chemiluminescent reaction, which results in the enhancement of light-emission from Coelenterazine itself. Thus, these results show the potential for the enhancement of chemiluminescent reactions by using CDs as catalysts. Future work would be needed to investigate the mechanism through which the CDs catalyze this type of reaction.

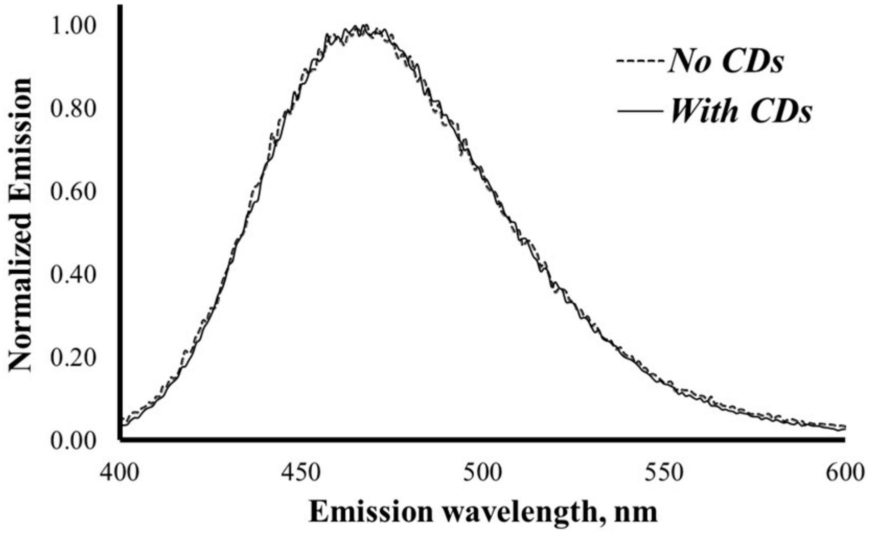

Figure 14. Normalized chemiluminescence spectra for Coelenterazine in DMSO, in the presence or absence of CDs. Spectra obtained with a Horiba Jovin Fluoromax 4 spectrofluorimeter, with a slit width of 29 nm for the emission monochromator.

Conclusion

This chapter focused on the use of CA for the making of CDs, with references to their synthetic procedures, properties, applications, doping mechanisms and results thereof, possible by-products, sustainability, and respective environmentally friendlier carbon source alternatives. CA is a versatile molecule naturally present in several fruits and vegetables, most important of which are citrus fruits. While it is used in many processes and applications, is CA is mostly known for its role in the Krebs cycle, which is of paramount importance for all aerobic organisms and a crucial part of obtaining food-derived energy in complex organisms. Regarding industrial applications, CA is used mostly in the food and beverage industry, and for a variety of other applications such as making bath salts, shampoos, degreasing agents, metal removal from water, rust removal, among others.

The low cost and characteristics of CA meant that it was a suitable carbon source for the synthesis of CDs, so much so that it is arguably the most commonly used precursor used to fabricate these nanoparticles. CDs are carbon-based nanoparticles that have been under the scope of the scientific community since their discovery in 2004. CDs can be synthesized via either top-down or bottom-up strategies, with the latter being more frequently employed due to its relative easiness and inexpensiveness. From the synthesis results a nanoparticle commonly presenting a carbogenic sp^2-hybridized core with a surface covered in functional groups (such as -OH). Among other properties, CDs are known to present a high photoluminescence, good water solubility, broadband absorption, and biocompatibility. From this results that CDs are suitable for a variety of applications in different fields, including bioimaging, photocatalysis, photodynamic therapy, sensing and light-emitting devices.

Additionally, the optoelectronic properties of CDs can be further enhanced by doping them with either heteroatoms or metallic dopants. Doping is a process that increases the particles' QY_{PL}, by prompting the formation of n- and p-type carriers (extra e^- and h^+), changing the CDs' electronic structure. The most commonly used dopant heteroatom in the synthesis of CDs is nitrogen, with combinations of CA with either urea or ethylenediamine (nitrogen-containing molecules) being extremely common for all kinds of CDs' applications. Other heteroatom dopants and combinations of dopants are also commonly used. Although metallic ions can also act as electron donors in CDs and enhance their electron transfer capacity (and ultimately extend the range of their applications), metallic doping is less common than its heteroatom counterpart. This may be attributed to the fact that metal-doped CDs present a relatively lower QY_{PL} and that their photoluminescence mechanism is still very unclear.

Among the properties of CDs, their photoluminescence is arguably the most important. However, the origins behind it are still a matter of debate, with several explanations and theories being presented by the scientific community over the years. The role of molecular by-products formed alongside the CDs during their synthesis has been under focus, as it was seen that these by-products are intensely photoluminescent, even more so than the nanoparticles themselves. In fact, the by-products might mask the nanoparticles' emission and, more importantly, they may even react with the CDs and alter their optical properties and photochemical reactivity. When co-existing in solution a synergistic effect may occur between CDs and by-products. Whereas this causes a need of a proper purification of the CDs after their synthesis, it also brings potential in terms of discovering new applications based on the hybrid photoluminescence and synergy between CDs and photoluminescent by-products.

Finally, the sustainability of using carbon sources such as CA for the synthesis of CDs was also reviewed. We found that the carbon source plays an important in the environmental impacts of the synthesis. Several LCA-based studies point that the carbon precursor quantity and, more importantly, the identity of the carbon precursor play a major role in determining the sustainability of the CDs' synthesis. Choosing a more sustainable and renewable alternative carbon precursor is an important step towards sustainability that is already being studied by several teams across the world. Several waste and biomass-based CDs have been reported over the last years, using precursors as varied as corn stover, spent coffee grounds, fish scales and milk, presenting properties in line with those of conventional CDs and capable of being employed in the same applications, all while also being much more sustainable, less expensive and promoting a circular economy. It was here also demonstrated a potential application of waste-based CDs in the catalysis of chemiluminescent reactions.

Acknowledgments

The Portuguese "*Fundação para a Ciência e Tecnologia* [Foundation for Science and Technology]" (FCT, Lisbon) is acknowledged for funding of project PTDC/QUI-QFI/2870/2020, R&D Unit CIQUP (UIDB/00081/2020), and Associated Laboratory IMS (LA/P/0056/ 2020). Luís Pinto da Silva acknowledges funding from FCT under the Scientific Employment Stimulus (CEECINST/00069/2021). The Materials Center of the University of Porto (CEMUP) is acknowledged. Ricardo Sendão acknowledges FCT for his Ph.D. grant (2021.06149.BD).

References

[1] Penniston, K. L., S. Y. Nakada, R. P. Holmes, and D. G. Assimos, Quantitative assessment of citric acid in lemon juice, lime juice, and commercially-available fruit juice products. *J. Endourol.*, 2008. 22(3): p. 567-70.

[2] Lotfy, W. A., K. M. Ghanem, and E. R. El-Helow, Citric acid production by a novel Aspergillus niger isolate: II. Optimization of process parameters through statistical experimental designs. *Bioresour. Technol.*, 2007. 98(18): p. 3470-7.

[3] Verhoff, F. H. and H. Bauweleers, *Ullmann's Encyclopedia of Industrial Chemistry*. 2014, Weinheim: Wiley-VCH.

[4] Amir, D., A. Hendler-Neumark, V. Wulf, R. Ehrlich, and G. Bisker, Oncometabolite Fingerprinting Using Fluorescent Single-Walled Carbon Nanotubes. *Adv. Mater. Interfaces*, 2021. 9(4).

[5] Abdullah, T. A., T. Juzsakova, S. A. Hafad, R. T. Rasheed, N. Al-Jammal, M. A. Mallah, A. D. Salman, P. C. Le, E. Domokos, and M. Aldulaimi, Functionalized multi-walled carbon nanotubes for oil spill cleanup from water. *Clean Technol. Environ. Policy*, 2021. 24(2): p. 519-541.

[6] Norouzi, A., E. Nemati Lay, A. Arabloo nareh, A. Hosseinkhani, and M. Chapalaghi, Functionalized nanodiamonds in polyurethane mixed matrix membranes for carbon dioxide separation. *Results in Materials*, 2022. 13.

[7] Chhetri, K., T. Kim, D. Acharya, A. Muthurasu, B. Dahal, R. M. Bhattarai, P. C. Lohani, I. Pathak, S. Ji, T. H. Ko, and H. Y. Kim, Hollow Carbon Nanofibers with Inside-outside Decoration of Bi-metallic MOF Derived Ni-Fe Phosphides as Electrode Materials for Asymmetric Supercapacitors. *Chem. Eng. J.*, 2022. 450.

[8] Lu, D., X. Shi, H. S. Wong, Z. Jiang, and J. Zhong, Graphene coated sand for smart cement composites. *Const. Build. Mater.*, 2022. 346.

[9] Jayanand, K., S. Chugh, N. Adhikari, M. Min, L. Echegoyen, and A. B. Kaul, Sc3N@C80 and La@C82 doped graphene for a new class of optoelectronic devices. *J. Mater. Chem. C*, 2020. 8: p. 3970.

[10] Zhu, Z., X. Li, M. Luo, M. Chen, W. Chen, P. Yang, and X. Zhou, Synthesis of carbon dots with high photocatalytic reactivity by tailoring heteroatom doping. *J. Colloid. Interface Sci.*, 2022. 605: p. 330-341.

[11] Smrithi, S. P., N. Kottam, and B. R. Vergis, Heteroatom Modified Hybrid Carbon Quantum Dots Derived from Cucurbita pepo for the Visible Light Driven Photocatalytic Dye Degradation. *Top. Catal.,* 2022.

[12] Simoes, E. F. C., L. P. da Silva, J. da Silva, and J. M. M. Leitao, Hypochlorite fluorescence sensing by phenylboronic acid-alizarin adduct based carbon dots. *Talanta*, 2020. 208: p. 120447.

[13] Ladomenou, K., G. Landrou, G. Charalambidis, E. Nikoloudakis, and A. G. Coutsolelos, Carbon dots for photocatalytic H2 production in aqueous media with molecular Co catalysts. *Sustain. Energy Fuels*, 2021. 5(2): p. 449-458.

[14] Li, L.-S. and L. Xu, Highly fluorescent N,S,P tri-doped carbon dots for Cl− detection and their assistance of TiO_2 as the catalyst in the degradation of methylene blue. *J. Photochem. Photobiol. A*, 2020. 401.

[15] Kalytchuk, S., K. Polakova, Y. Wang, J. P. Froning, K. Cepe, A. L. Rogach, and R. Zboril, Carbon Dot Nanothermometry: Intracellular Photoluminescence Lifetime Thermal Sensing. *ACS Nano*, 2017. 11(2): p. 1432-1442.

[16] Xu, X., R. Ray, Y. Gu, H. J. Ploehn, L. Gearheart, K. Raker, and W. A. Scrivens, Electrophoretic analysis and purification of fluorescent single-walled carbon nanotube fragments. *J. Am. Chem. Soc.*, 2004. 126(40): p. 12736-7.

[17] Sun, Y. P., B. Zhou, Y. Lin, W. Wang, K. A. Fernando, P. Pathak, M. J. Meziani, B. A. Harruff, X. Wang, H. Wang, P. G. Luo, H. Yang, M. E. Kose, B. Chen, L. M. Veca, and S. Y. Xie, Quantum-sized carbon dots for bright and colorful photoluminescence. *J. Am. Chem. Soc.*, 2006. 128(24): p. 7756-7.

[18] Esteves da Silva, J. C. G. and H. M. R. Gonçalves, Analytical and bioanalytical applications of carbon dots. *Trends Analyt. Chem.*, 2011. 30(8): p. 1327-1336.

[19] Hola, K., Y. Zhang, Y. Wang, E. P. Giannelis, R. Zboril, and A. L. Rogach, Carbon dots—Emerging light emitters for bioimaging, cancer therapy and optoelectronics. *Nano Today*, 2014. 9(5): p. 590-603.

[20] Baker, S. N. and G. A. Baker, Luminescent carbon nanodots: emergent nanolights. *Angew. Chem. Int. Ed. Engl.*, 2010. 49(38): p. 6726-44.

[21] Demchenko, A. P. and M. O. Dekaliuk, Novel fluorescent carbonic nanomaterials for sensing and imaging. *Methods Appl. Fluoresc.*, 2013. 1(4): p. 042001.

[22] Sendão, R. M. S., D. M. A. Crista, A. C. P. Afonso, M. D. V. Martinez de Yuso, M. Algarra, J. C. G. Esteves da Silva, and L. Pinto da Silva, Insight into the hybrid luminescence showed by carbon dots and molecular fluorophores in solution. *Phys. Chem. Chem. Phys.*, 2019. 21(37): p. 20919-20926.

[23] Wang, J., S. Sahu, S. K. Sonkar, K. N. Tackett Ii, K. W. Sun, Y. Liu, H. Maimaiti, P. Anilkumar, and Y.-P. Sun, Versatility with carbon dots – from overcooked BBQ to brightly fluorescent agents and photocatalysts. *RSC Adv.*, 2013. 3(36).

[24] Saini, D., J. Kaushik, A. K. Garg, C. Dalal, and S. K. Sonkar, N, S-codoped Carbon Dots for Nontoxic Cell Imaging and As a Sunlight-Active Photocatalytic Material for the Removal of Chromium. *ACS Appl. Bio. Mater.*, 2020. 3(6): p. 3656-3663.

[25] Vale, N., S. Silva, D. Duarte, D. M. A. Crista, L. Pinto da Silva, and J. C. G. Esteves da Silva, Normal breast epithelial MCF-10A cells to evaluate the safety of carbon dots. *RSC Med. Chem.*, 2021. 12(2): p. 245-253.

[26] Hettiarachchi, S. D., R. M. Graham, K. J. Mintz, Y. Zhou, S. Vanni, Z. Peng, and R. M. Leblanc, Triple conjugated carbon dots as a nano-drug delivery model for glioblastoma brain tumors. *Nanoscale*, 2019. 11(13): p. 6192-6205.

[27] Deng, Y., M. Chen, G. Chen, W. Zou, Y. Zhao, H. Zhang, and Q. Zhao, Visible-Ultraviolet Upconversion Carbon Quantum Dots for Enhancement of the Photocatalytic Activity of Titanium Dioxide. *ACS Omega*, 2021. 6(6): p. 4247-4254.

[28] Gu, S., C.-T. Hsieh, Y.-M. Chiang, D.-Y. Tzou, Y.-F. Chen, and Y. A. Gandomi, Optimization of graphene quantum dots by chemical exfoliation from graphite powders and carbon nanotubes. *Mater. Chem. Phys.*, 2018. 215: p. 104-111.

[29] Zhuo, S., M. Shao, and S. T. Lee, Upconversion and downconversion fluorescent graphene quantum dots: ultrasonic preparation and photocatalysis. *ACS Nano*, 2012. 6(2): p. 1059-64.

[30] Zhou, J., C. Booker, R. Li, X. Zhou, T. K. Sham, X. Sun, and Z. Ding, An electrochemical avenue to blue luminescent nanocrystals from multiwalled carbon nanotubes (MWCNTs). *J. Am. Chem. Soc.*, 2007. 129(4): p. 744-5.

[31] Sendão, R., M. d. V. M. d. Yuso, M. Algarra, J. C. G. Esteves da Silva, and L. Pinto da Silva, Comparative life cycle assessment of bottom-up synthesis routes for carbon dots derived from citric acid and urea. *J. Clean. Prod.*, 2020. 254.

[32] Crista, D. M. A., G. P. C. Mello, O. Shevchuk, R. M. S. Sendao, E. F. C. Simoes, J. M. M. Leitao, L. P. da Silva, and J. C. G. Esteves da Silva, 3-Hydroxyphenylboronic Acid-Based Carbon Dot Sensors for Fructose Sensing. *J. Fluoresc.*, 2019. 29(1): p. 265-270.

[33] Campalani, C., E. Cattaruzza, S. Zorzi, A. Vomiero, S. You, L. Matthews, M. Capron, C. Mondelli, M. Selva, and A. Perosa, Biobased Carbon Dots: From Fish Scales to Photocatalysis. *Nanomaterials*, 2021. 11(2).

[34] Christe, S., J. C. G. Esteves da Silva, and L. Pinto da Silva, Evaluation of the Environmental Impact and Efficiency of N-Doping Strategies in the Synthesis of Carbon Dots. *Materials*, 2020. 13(3).

[35] Zhu, H., X. Wang, Y. Li, Z. Wang, F. Yang, and X. Yang, Microwave synthesis of fluorescent carbon nanoparticles with electrochemiluminescence properties. *Chem. Commun.*, 2009(34): p. 5118-20.

[36] Gu, Z. G., D. J. Li, C. Zheng, Y. Kang, C. Woll, and J. Zhang, MOF-Templated Synthesis of Ultrasmall Photoluminescent Carbon-Nanodot Arrays for Optical Applications. *Angew. Chem. Int. Ed. Engl.*, 2017. 56(24): p. 6853-6858.

[37] Jiang, H., F. Chen, M. G. Lagally, and F. S. Denes, New strategy for synthesis and functionalization of carbon nanoparticles. *Langmuir*, 2010. 26(3): p. 1991-5.

[38] Krysmann, M. J., A. Kelarakis, P. Dallas, and E. P. Giannelis, Formation mechanism of carbogenic nanoparticles with dual photoluminescence emission. *J. Am. Chem. Soc.*, 2012. 134(2): p. 747-50.

[39] Crista, D. M. A., J. C. G. Esteves da Silva, and L. Pinto da Silva, Evaluation of Different Bottom-up Routes for the Fabrication of Carbon Dots. *Nanomaterials*, 2020. 10(7).

[40] Peng, Z., Y. Zhou, C. Ji, J. Pardo, K. J. Mintz, R. R. Pandey, C. C. Chusuei, R. M. Graham, G. Yan, and R. M. Leblanc, Facile Synthesis of "Boron-Doped" Carbon Dots and Their Application in Visible-Light-Driven Photocatalytic Degradation of Organic Dyes. *Nanomaterials*, 2020. 10(8).

[41] Zhou, Y., E. M. Zahran, B. A. Quiroga, J. Perez, K. J. Mintz, Z. Peng, P. Y. Liyanage, R. R. Pandey, C. C. Chusuei, and R. M. Leblanc, Size-Dependent Photocatalytic Activity of Carbon Dots with Surface-State Determined Photoluminescence. *Appl. Catal. B*, 2019. 248: p. 157-166.

[42] Tan, J., R. Zou, J. Zhang, W. Li, L. Zhang, and D. Yue, Large-scale synthesis of N-doped carbon quantum dots and their phosphorescence properties in a polyurethane matrix. *Nanoscale*, 2016. 8(8): p. 4742-7.

[43] Qu, S., X. Wang, Q. Lu, X. Liu, and L. Wang, A biocompatible fluorescent ink based on water-soluble luminescent carbon nanodots. *Angew. Chem. Int. Ed. Engl.*, 2012. 51(49): p. 12215-8.

[44] Jiang, J., Y. He, S. Li, and H. Cui, Amino acids as the source for producing carbon nanodots: microwave assisted one-step synthesis, intrinsic photoluminescence property and intense chemiluminescence enhancement. *Chem. Commun.*, 2012. 48(77): p. 9634-6.

[45] Yang, Z. C., M. Wang, A. M. Yong, S. Y. Wong, X. H. Zhang, H. Tan, A. Y. Chang, X. Li, and J. Wang, Intrinsically fluorescent carbon dots with tunable

emission derived from hydrothermal treatment of glucose in the presence of monopotassium phosphate. *Chem. Commun.*, 2011. 47(42): p. 11615-7.

[46] De, B. and N. Karak, A green and facile approach for the synthesis of water soluble fluorescent carbon dots from banana juice. *RSC Adv.*, 2013. 3(22).

[47] Wang, L. and H. S. Zhou, Green synthesis of luminescent nitrogen-doped carbon dots from milk and its imaging application. *Anal. Chem.*, 2014. 86(18): p. 8902-5.

[48] Dong, Y., H. Pang, H. B. Yang, C. Guo, J. Shao, Y. Chi, C. M. Li, and T. Yu, Carbon-based dots co-doped with nitrogen and sulfur for high quantum yield and excitation-independent emission. *Angew. Chem. Int. Ed. Engl.*, 2013. 52(30): p. 7800-4.

[49] Schneider, J., C. J. Reckmeier, Y. Xiong, M. von Seckendorff, A. S. Susha, P. Kasák, and A. L. Rogach, Molecular Fluorescence in Citric Acid-Based Carbon Dots. *J. Phys. Chem. C*, 2017. 121(3): p. 2014-2022.

[50] Kasprzyk, W., S. Bednarz, P. Żmudzki, M. Galica, and D. Bogdał, Novel efficient fluorophores synthesized from citric acid. *RSC Adv.*, 2015. 5(44): p. 34795-34799.

[51] Fang, Q., Y. Dong, Y. Chen, C.-H. Lu, Y. Chi, H.-H. Yang, and T. Yu, Luminescence origin of carbon based dots obtained from citric acid and amino group-containing molecules. *Carbon*, 2017. 118: p. 319-326.

[52] Belkahla, H., R. Boudjemaa, V. Caorsi, D. Pineau, A. Curcio, J. S. Lomas, P. Decorse, A. Chevillot-Biraud, T. Azaïs, C. Wilhelm, H. Randriamahazaka, and M. Hémadi, Carbon dots, a powerful non-toxic support for bioimaging by fluorescence nanoscopy and eradication of bacteria by photothermia. *Nanoscale Adv.*, 2019. 1(7): p. 2571-2579.

[53] Li, J., K. Tang, J. Yu, H. Wang, M. Tu, and X. Wang, Nitrogen and chlorine co-doped carbon dots as probe for sensing and imaging in biological samples. *R. Soc. Open Sci.,* 2019. 6(1): p. 181557.

[54] Kong, T., L. Hao, Y. Wei, X. Cai, and B. Zhu, Doxorubicin conjugated carbon dots as a drug delivery system for human breast cancer therapy. *Cell Prolif.*, 2018. 51(5): p. e12488.

[55] Yang, K., C. Wang, C. Liu, S. Ding, F. Tian, and F. Li, Bioluminescence-initiated photodynamic therapy bridged on high-luminescent carbon dots-conjugated protoporphyrin IX. *J. Mater. Sci.*, 2019. 54(4): p. 3383-3391.

[56] Yang, K., C. Wang, X. Wei, S. Ding, C. Liu, F. Tian, and F. Li, Self-Illuminating Photodynamic Therapy with Enhanced Therapeutic Effect by Optimization of the Chemiluminescence Resonance Energy Transfer Step to the Photosensitizer. *Bioconjug. Chem.*, 2020. 31(3): p. 595-604.

[57] An, Y., C. Liu, Y. Li, M. Chen, Y. Zheng, H. Tian, R. Shi, X. He, and X. Lin, Preparation of Multicolour Solid Fluorescent Carbon Dots for Light-Emitting Diodes Using Phenylethylamine as a Co-Carbonization Agent. *Int. J. Mol. Sci.*, 2022. 23(19).

[58] Yuan, F., Y.-K. Wang, G. Sharma, Y. Dong, X. Zheng, P. Li, A. Johnston, G. Bappi, J. Z. Fan, H. Kung, B. Chen, M. I. Saidaminov, K. Singh, O. Voznyy, O. M. Bakr, Z.-H. Lu, and E. H. Sargent, Bright high-colour-purity deep-blue carbon dot light-emitting diodes via efficient edge amination. *Nat. Photon.*, 2019. 14(3): p. 171-176.

[59] Aggarwal, R., D. Saini, S. K. Sonkar, A. K. Sonker, and G. Westman, Sunlight promoted removal of toxic hexavalent chromium by cellulose derived photoactive carbon dots. *Chemosphere*, 2022. 287(Pt 3): p. 132287.

[60] Huang, P., S. Xu, M. Zhang, W. Zhong, Z. Xiao, and Y. Luo, Green carbon dots based ultraviolet photovoltaic window with high transparence to visible light. *Int. J. Energy Res.*, 2021. 45(12): p. 17709-17720.

[61] Ansón-Casaos, A., J. Hernández-Ferrer, L. Vallan, H. Xie, M. Lira-Cantú, A. M. Benito, and W. K. Maser, Functionalized carbon dots on TiO_2 for perovskite photovoltaics and stable photoanodes for water splitting. *Int. J. Hydrog. Energy*, 2021. 46(22): p. 12180-12191.

[62] Fiori, F., H. Moukham, F. Olia, D. Piras, S. Ledda, A. Salis, L. Stagi, L. Malfatti, and P. Innocenzi, Highly Photostable Carbon Dots from Citric Acid for Bioimaging. *Materials*, 2022. 15(7).

[63] Ding, H., J. S. Wei, N. Zhong, Q. Y. Gao, and H. M. Xiong, Highly Efficient Red-Emitting Carbon Dots with Gram-Scale Yield for Bioimaging. *Langmuir*, 2017. 33(44): p. 12635-12642.

[64] Bhaisare, M. L., A. Talib, M. S. Khan, S. Pandey, and H.-F. Wu, Synthesis of fluorescent carbon dots via microwave carbonization of citric acid in presence of tetraoctylammonium ion, and their application to cellular bioimaging. *Microchim. Acta*, 2015. 182(13-14): p. 2173-2181.

[65] Wan, J., S. Xu, J. Li, M. Yu, K. Zhang, G. Wei, and Z. Su, Facile synthesis of multifunctional pharmaceutical carbon dots for targeted bioimaging and chemotherapy of tumors. *Nanoscale*, 2022. 14(31): p. 11359-11368.

[66] Li, S., X. Song, Z. Hu, and G. Feng, A carbon dots-based ratiometric fluorescence probe for monitoring intracellular pH and bioimaging. *J. Photochem. Photobiol. A*, 2021. 409.

[67] Wang, L., B. Wang, E. Liu, Y. Zhao, B. He, C. Wang, G. Xing, Z. Tang, Y. Zhou, and S. Qu, Polyetherimide functionalized carbon dots with enhanced red emission in aqueous solution for bioimaging. *Chin. Chem. Lett.*, 2022. 33(8): p. 4111-4115.

[68] Shan, F., H. Xia, X. Xie, L. Fu, H. Yang, Q. Zhou, Y. Zhang, Z. Wang, and X. Yu, Novel N-doped carbon dots prepared via citric acid and benzoylurea by green synthesis for high selectivity Fe(III) sensing and imaging in living cells. *Microchem. J.*, 2021. 167.

[69] Wang, Q., L. Shi, J. Zhao, and S. Shuang, Fluorescent carbon dots with real-time nucleolus-monitoring capability for gene delivery and biosensing of NO2– and pH. *Appl. Surf. Sci.*, 2022. 599.

[70] Singaravelu, C. M., X. Deschanels, C. Rey, and J. Causse, Solid-State Fluorescent Carbon Dots for Fluorimetric Sensing of Hg2+. *ACS Appl. Nano Mater.*, 2021. 4(6): p. 6386-6397.

[71] Bogireddy, N. K. R., S. E. Sotelo Rios, and V. Agarwal, Simple one step synthesis of dual-emissive heteroatom doped carbon dots for acetone sensing in commercial products and Cr (VI) reduction. *Chem. Eng. J.,* 2021. 414.

[72] Zhou, Y., S. Zhang, S. Li, L. Wei, and L. Zhang, Multifunctional N doped carbon dots for cellular sensing, light-emitting-diode, and additive manufacturing. *Mater. Lett.*, 2022. 325.

[73] Lin, Z., Q. Zeng, Q. Deng, W. Yao, H. Deng, X. Lin, and W. Chen, Citric acid-derived carbon dots as excellent cysteine oxidase mimics for cysteine sensing. *Sens. Actuators B Chem.*, 2022. 359.

[74] Hu, Q., W. Wang, Z. Q. Yang, L. Xiao, X. Gong, L. Liu, and J. Han, An ultrasensitive sensing platform based on fluorescence carbon dots for chlorogenic acid determination in food samples. *Food Chem.*, 2023. 404(Pt A): p. 134395.

[75] Zou, G.-Y., L. Guo, S. Chen, N.-Z. Liu, and Y.-L. Yu, Multifunctional ratiometric fluorescent sensing platform constructed by grafting various response groups on carbon dots with bromine active site for biosensing and bioimaging. *Sens. Actuators B Chem.*, 2022. 357.

[76] Zeng, Q., D. Shao, X. He, Z. Ren, W. Ji, C. Shan, S. Qu, J. Li, L. Chen, and Q. Li, Carbon dots as a trackable drug delivery carrier for localized cancer therapy in vivo. *J. Mater. Chem. B*, 2016. 4(30): p. 5119-5126.

[77] Peng, Z., E. H. Miyanji, Y. Zhou, J. Pardo, S. D. Hettiarachchi, S. Li, P. L. Blackwelder, I. Skromne, and R. M. Leblanc, Carbon dots: promising biomaterials for bone-specific imaging and drug delivery. *Nanoscale*, 2017. 9(44): p. 17533-17543.

[78] Pandey, A., A. Devkota, A. Sigdel, Z. Yadegari, K. Dumenyo, and A. Taheri, Citric acid/beta-alanine carbon dots as a novel tool for delivery of plasmid DNA into E. coli cells. *Sci. Rep.*, 2021. 11(1): p. 23964.

[79] Zhou, Y., P. Y. Liyanage, D. Devadoss, L. R. Rios Guevara, L. Cheng, R. M. Graham, H. S. Chand, A. O. Al-Youbi, A. S. Bashammakh, M. S. El-Shahawi, and R. M. Leblanc, Nontoxic amphiphilic carbon dots as promising drug nanocarriers across the blood-brain barrier and inhibitors of beta-amyloid. *Nanoscale*, 2019. 11(46): p. 22387-22397.

[80] Suner, S. S., M. Sahiner, A. S. Yilmaz, R. S. Ayyala, and N. Sahiner, Light-Activated Modified Arginine Carbon Dots as Antibacterial Particles. *Catalysts*, 2022. 12(11).

[81] Lv, Y., P. Li, R. Su, J. Cai, H. Zhong, F. Wen, and W. Su, Methylene Blue/Carbon Dots Composite with Photothermal and Photodynamic Properties: Synthesis, Characterization, and Antibacterial Application. *Photochem. Photobiol.*, 2022.

[82] Romero, M. P., F. Alves, M. D. Stringasci, H. H. Buzza, H. Ciol, N. M. Inada, and V. S. Bagnato, One-Pot Microwave-Assisted Synthesis of Carbon Dots and in vivo and in vitro Antimicrobial Photodynamic Applications. *Front. Microbiol.*, 2021. 12: p. 662149.

[83] Kong, T., T. Liu, Y. Zhang, and M. Wang, Carbon dots with intrinsic theranostic properties for photodynamic therapy of oral squamous cell carcinoma. *J. Biomater. Appl.*, 2022. 37(5): p. 850-858.

[84] Yang, Y., H. Ding, Z. Li, A. C. Tedesco, and H. Bi, Carbon Dots Derived from Tea Polyphenols as Photosensitizers for Photodynamic Therapy. *Molecules*, 2022. 27(23).

[85] Wang, H. J., W. Y. Hou, Y. W. Hao, W. S. Jiang, H. L. Chen, and Q. Q. Zhang, Novel yellow solid-state fluorescent-emitting carbon dots with high quantum yield for white light-emitting diodes. *Spectrochim. Acta A Mol. Biomol. Spectrosc.*, 2021. 250: p. 119340.

[86] Qiu, H., F. Yuan, Y. Wang, Z. Zhang, J. Li, and Y. Li, Green-light-emitting carbon dots via eco-friendly route and their potential in ferric-ion detection and WLEDs. *Mater. Adv.*, 2022. 3(19): p. 7339-7347.

[87] Yang, X., L. Sui, B. Wang, Y. Zhang, Z. Tang, B. Yang, and S. Lu, Red-emitting, self-oxidizing carbon dots for the preparation of white LEDs with super-high color rendering index. *Sci. China Chem.*, 2021. 64(9): p. 1547-1553.

[88] Zhang, C., T. Lin, X. Yin, X. Wu, and X. Wei, Preparation of transparent wood containing carbon dots for application in the field of white-LED. *J. Wood Chem. Technol.*, 2022. 42(5): p. 331-341.

[89] Zhang, J., D. Nan, S. Pan, H. Liu, H. Yang, and X. Hu, N,S co-doped carbon dots as a dual-functional fluorescent sensor for sensitive detection of baicalein and temperature. *Spectrochim. Acta A Mol. Biomol. Spectrosc.*, 2019. 221: p. 117161.

[90] Zuo, P., J. Liu, H. Guo, C. Wang, H. Liu, Z. Zhang, and Q. Liu, Multifunctional N,S co-doped carbon dots for sensitive probing of temperature, ferric ion, and methotrexate. *Anal. Bioanal. Chem.*, 2019. 411(8): p. 1647-1657.

[91] Zhang, H., J. You, J. Wang, X. Dong, R. Guan, and D. Cao, Highly luminescent carbon dots as temperature sensors and “off-on” sensing of Hg^{2+} and biothiols. *Dyes Pigm.*, 2020. 173.

[92] Sendão, R. M. S., J. C. G. Esteves da Silva, and L. Pinto da Silva, Applications of Fluorescent Carbon Dots as Photocatalysts: A Review. *Catalysts*, 2023. 13(1).

[93] Jana, B., Y. Reva, T. Scharl, V. Strauss, A. Cadranel, and D. M. Guldi, Carbon Nanodots for All-in-One Photocatalytic Hydrogen Generation. *J. Am. Chem. Soc.*, 2021. 143(48): p. 20122-20132.

[94] Zhou, Y., A. E. ElMetwally, J. Chen, W. Shi, E. K. Cilingir, B. Walters, K. J. Mintz, C. Martin, B. Ferreira, W. Zhang, S. D. Hettiarachchi, L. F. Serafim, P. L. Blackwelder, A. H. Wikramanayake, Z. Peng, and R. M. Leblanc, Gel-like carbon dots: A high-performance future photocatalyst. *J. Colloid Interface Sci.*, 2021. 599: p. 519-532.

[95] Nabid, M. R., Y. Bide, and N. Fereidouni, Boron and nitrogen co-doped carbon dots as a metal-free catalyst for hydrogen generation from sodium borohydride. *New J. Chem.*, 2016. 40(10): p. 8823-8828.

[96] Al-Azmi, A. and S. Keshipour, New bidental sulfur-doped graphene quantum dots modified with gold as a catalyst for hydrogen generation. *J. Colloid Interface Sci.*, 2022. 612: p. 701-709.

[97] Aghamali, A., M. Khosravi, H. Hamishehkar, N. Modirshahla, and M. A. Behnajady, Synthesis and characterization of high efficient photoluminescent sunlight driven photocatalyst of N-Carbon Quantum Dots. *J. Lumin.*, 2018. 201: p. 265-274.

[98] Amadio, E., S. Cailotto, C. Campalani, L. Branzi, C. Raviola, D. Ravelli, E. Cattaruzza, E. Trave, A. Benedetti, M. Selva, and A. Perosa, Precursor-Dependent Photocatalytic Activity of Carbon Dots. *Molecules*, 2019. 25(1).

[99] Kaushal, N., A. L. Sharma, and A. Saha, Visible LED-based photo-redox properties of sulfur and nitrogen-doped carbon dots designed by solid-state synthesis. *Mater. Adv.*, 2022. 3(1): p. 355-361.

[100] Lim, H., Y. Liu, H. Y. Kim, and D. I. Son, Facile synthesis and characterization of carbon quantum dots and photovoltaic applications. *Thin Solid Films*, 2018. 660: p. 672-677.

[101] Bora, A., K. Mohan, and S. K. Dolui, Carbon Dots as Cosensitizers in Dye-Sensitized Solar Cells and Fluorescence Chemosensors for 2,4,6-Trinitrophenol Detection. *Ind. Eng. Chem. Res.*, 2019. 58(51): p. 22771-22778.

[102] Efa, M. T. and T. Imae, Effects of carbon dots on ZnO nanoparticle-based dye-sensitized solar cells. *Electrochim. Acta*, 2019. 303: p. 204-210.

[103] Zhang, X., J. Lu, X. Zhou, C. Guo, and C. Wang, Rapid microwave synthesis of N-doped carbon nanodots with high fluorescence brightness for cell imaging and sensitive detection of iron (III). *Opt. Mater.*, 2017. 64: p. 1-8.

[104] Zhang, Z., G. Yi, P. Li, X. Zhang, H. Fan, X. Wang, C. Zhang, Y. Zhang, and Q. Sun, Construction of N-Doped Carbon Dots/Macroporous TiO_2 Composites (N-CDs/m-TiO_2) with Dramatically Enhanced Photocatalytic Activity. *Ind. Eng. Chem. Res.,* 2021. 60(32): p. 11954-11963.

[105] Huang, B., J. He, S. Bian, C. Zhou, Z. Li, F. Xi, J. Liu, and X. Dong, S-doped graphene quantum dots as nanophotocatalyst for visible light degradation. *Chin. Chem. Lett.*, 2018. 29(11): p. 1698-1701.

[106] Bhati, A., S. R. Anand, D. Saini, Gunture, and S. K. Sonkar, Sunlight-induced photoreduction of Cr(VI) to Cr(III) in wastewater by nitrogen-phosphorus-doped carbon dots. *NPJ Clean Water*, 2019. 2(1).

[107] Guo, Z., H. Wu, M. Li, T. Tang, J. Wen, and X. Li, Phosphorus-doped graphene quantum dots loaded on TiO_2 for enhanced photodegradation. *Appl. Surf. Sci.*, 2020. 526.

[108] Li, L. and T. Dong, Photoluminescence tuning in carbon dots: surface passivation or/and functionalization, heteroatom doping. *J. Mater. Chem. C*, 2018. 6(30): p. 7944-7970.

[109] Mombrú, D., M. Romero, R. Faccio, and Á. W. Mombrú, Electronic and optical properties of sulfur and nitrogen doped graphene quantum dots: A theoretical study. *Physica E Low dimens. Syst. Nanostruct.*, 2019. 113: p. 130-136.

[110] Lou, Z., S. Zhao, Q. Wang, and H. Wei, N-Doped Carbon As Peroxidase-Like Nanozymes for Total Antioxidant Capacity Assay. *Anal. Chem.*, 2019. 91(23): p. 15267-15274.

[111] Lee, A., S. Yun, E. S. Kang, J. W. Kim, J. H. Park, and J. S. Choi, Effect of heteroatoms on the optical properties and enzymatic activity of N-doped carbon dots. *RSC Adv.*, 2021. 11(31): p. 18776-18782.

[112] Miao, X., D. Qu, D. Yang, B. Nie, Y. Zhao, H. Fan, and Z. Sun, Synthesis of Carbon Dots with Multiple Color Emission by Controlled Graphitization and Surface Functionalization. *Adv. Mater.*, 2018. 30(1).

[113] Hien, N. T., T. T. K. Chi, N. D. Vinh, H. T. Van, L. D. Thanh, P. V. Do, V. P. Tuyen, and N. X. Ca, Synthesis, characterization and the photoinduced electron-transfer energetics of CdTe/CdSe type-II core/shell quantum dots. *J. Lumin.*, 2020. 217.

[114] Sun, H., A. Zhao, N. Gao, K. Li, J. Ren, and X. Qu, Deciphering a nanocarbon-based artificial peroxidase: chemical identification of the catalytically active and

substrate-binding sites on graphene quantum dots. *Angew. Chem. Int. Ed. Engl.*, 2015. 54(24): p. 7176-80.

[115] Wibrianto, A., S. Q. Khairunisa, S. C. W. Sakti, Y. L. Ni'mah, B. Purwanto, and M. Z. Fahmi, Comparison of the effects of synthesis methods of B, N, S, and P-doped carbon dots with high photoluminescence properties on HeLa tumor cells. *RSC Adv.*, 2020. 11(2): p. 1098-1108.

[116] Zhu, S., Y. Song, X. Zhao, J. Shao, J. Zhang, and B. Yang, The photoluminescence mechanism in carbon dots (graphene quantum dots, carbon nanodots, and polymer dots): current state and future perspective. *Nano Res.*, 2015. 8(2): p. 355-381.

[117] Xia, C., S. Zhu, T. Feng, M. Yang, and B. Yang, Evolution and Synthesis of Carbon Dots: From Carbon Dots to Carbonized Polymer Dots. *Adv. Sci.*, 2019. 6(23): p. 1901316.

[118] Kim, T., J. Lee, and K.-H. Lee, Microwave heating of carbon-based solid materials. *Carbon Lett.,* 2014. 15(1): p. 15-24.

[119] Liang, C., Y. Wang, and T. Li, Synthesis of sulfur-doped p-type graphene by annealing with hydrogen sulfide. *Carbon*, 2015. 82: p. 506-512.

[120] Xu, Q., W. Cai, M. Zhang, R. Su, Y. Ye, Y. Li, L. Zhang, Y. Guo, Z. Yu, S. Li, X. Lin, Y. Chen, Y. Luo, J. Street, and M. Xu, Photoluminescence mechanism and applications of Zn-doped carbon dots. *RSC Adv.*, 2018. 8(31): p. 17254-17262.

[121] Gencer, O., Ö. F. Çeven, and C. Ünlü, Triggering excitation independent fluorescence in zinc(II) incorporated carbon dots: Surface passivation of carbon dots with zinc(II) ions by microwave assisted synthesis methods. *Diam. Relat. Mater.*, 2022. 123.

[122] Zhuo, S., J. Fang, M. Li, J. Wang, C. Zhu, and J. Du, Manganese(II)-doped carbon dots as effective oxidase mimics for sensitive colorimetric determination of ascorbic acid. *Mikrochim. Acta*, 2019. 186(12): p. 745.

[123] Ma, Y., Y. Cen, M. Sohail, G. Xu, F. Wei, M. Shi, X. Xu, Y. Song, Y. Ma, and Q. Hu, A Ratiometric Fluorescence Universal Platform Based on N, Cu Codoped Carbon Dots to Detect Metabolites Participating in H(2)O(2)-Generation Reactions. *ACS Appl. Mater. Interfaces*, 2017. 9(38): p. 33011-33019.

[124] Liu, J., Q. Chen, Z. Zhang, Z. Wang, and Z. Gong, Nitrogen and copper (II) co-doped carbon dots as multi-functional fluorescent probes for Fe3+ ions and tetracycline. *Microchem. J.*, 2022. 181.

[125] Kumar, V. B., R. Kumar, A. Gedanken, and O. Shefi, Fluorescent metal-doped carbon dots for neuronal manipulations. *Ultrason. Sonochem.*, 2019. 52: p. 205-213.

[126] Jiang, K., S. Sun, L. Zhang, Y. Lu, A. Wu, C. Cai, and H. Lin, Red, green, and blue luminescence by carbon dots: full-color emission tuning and multicolor cellular imaging. *Angew. Chem. Int. Ed. Engl.*, 2015. 54(18): p. 5360-3.

[127] Tang, L., R. Ji, X. Cao, J. Lin, H. Jiang, X. Li, K. S. Teng, C. M. Luk, S. Zeng, J. Hao, and S. P. Lau, Deep ultraviolet photoluminescence of water-soluble self-passivated graphene quantum dots. *ACS Nano*, 2012. 6(6): p. 5102-10.

[128] Xiao, L., Y. Wang, Y. Huang, T. Wong, and H. Sun, Self-trapped exciton emission from carbon dots investigated by polarization anisotropy of photoluminescence and photoexcitation. *Nanoscale*, 2017. 9(34): p. 12637-12646.

[129] Ghosh, S., A. M. Chizhik, N. Karedla, M. O. Dekaliuk, I. Gregor, H. Schuhmann, M. Seibt, K. Bodensiek, I. A. Schaap, O. Schulz, A. P. Demchenko, J. Enderlein, and A. I. Chizhik, Photoluminescence of carbon nanodots: dipole emission centers and electron-phonon coupling. *Nano Lett.*, 2014. 14(10): p. 5656-61.

[130] Demchenko, A. P. and M. O. Dekaliuk, The origin of emissive states of carbon nanoparticles derived from ensemble-averaged and single-molecular studies. *Nanoscale*, 2016. 8(29): p. 14057-69.

[131] Essner, J. B., J. A. Kist, L. Polo-Parada, and G. A. Baker, Artifacts and Errors Associated with the Ubiquitous Presence of Fluorescent Impurities in Carbon Nanodots. *Chem. Mater.,* 2018. 30(6): p. 1878-1887.

[132] Kasprzyk, W., T. Swiergosz, S. Bednarz, K. Walas, N. V. Bashmakova, and D. Bogdal, Luminescence phenomena of carbon dots derived from citric acid and urea - a molecular insight. *Nanoscale*, 2018. 10(29): p. 13889-13894.

[133] Ren, J., F. Weber, F. Weigert, Y. Wang, S. Choudhury, J. Xiao, I. Lauermann, U. Resch-Genger, A. Bande, and T. Petit, Influence of surface chemistry on optical, chemical and electronic properties of blue luminescent carbon dots. *Nanoscale*, 2019. 11(4): p. 2056-2064.

[134] Fadeel, B., C. Bussy, S. Merino, E. Vazquez, E. Flahaut, F. Mouchet, L. Evariste, L. Gauthier, A. J. Koivisto, U. Vogel, C. Martin, L. G. Delogu, T. Buerki-Thurnherr, P. Wick, D. Beloin-Saint-Pierre, R. Hischier, M. Pelin, F. Candotto Carniel, M. Tretiach, F. Cesca, F. Benfenati, D. Scaini, L. Ballerini, K. Kostarelos, M. Prato, and A. Bianco, Safety Assessment of Graphene-Based Materials: Focus on Human Health and the Environment. *ACS Nano*, 2018. 12(11): p. 10582-10620.

[135] Hischier, R. and T. Walser, Life cycle assessment of engineered nanomaterials: state of the art and strategies to overcome existing gaps. *Sci. Total Environ.*, 2012. 425: p. 271-82.

[136] Ramos, A., C. A. Teixeira, and A. Rouboa, Assessment study of an advanced gasification strategy at low temperature for syngas generation. *Int. J. Hydrog. Energy*, 2018. 43(21): p. 10155-10166.

[137] Fernandes, S., J. C. G. Esteves da Silva, and L. Pinto da Silva, Comparative life cycle assessment of high-yield synthesis routes for carbon dots. *NanoImpact*, 2021. 23.

[138] Pourzahedi, L. and M. J. Eckelman, Comparative life cycle assessment of silver nanoparticle synthesis routes. *Environ. Sci. Nano*, 2015. 2(4): p. 361-369.

[139] Algarra, M., L. d. Orfãos, C. S. Alves, R. Moreno-Tost, M. S. Pino-González, J. Jiménez-Jiménez, E. Rodríguez-Castellón, D. Eliche-Quesada, E. Castro, and R. Luque, Sustainable Production of Carbon Nanoparticles from Olive Pit Biomass: Understanding Proton Transfer in the Excited State on Carbon Dots. *ACS Sustain. Chem. Eng.*, 2019. 7(12): p. 10493-10500.

[140] Jing, S., Y. Zhao, R.-C. Sun, L. Zhong, and X. Peng, Facile and High-Yield Synthesis of Carbon Quantum Dots from Biomass-Derived Carbons at Mild Condition. *ACS Sustain. Chem. Eng.*, 2019. 7(8): p. 7833-7843.

[141] Crista, D. M. A., A. El Mragui, M. Algarra, J. C. G. Esteves da Silva, R. Luque, and L. Pinto da Silva, Turning Spent Coffee Grounds into Sustainable Precursors for the Fabrication of Carbon Dots. *Nanomaterials*, 2020. 10(6).

[142] Dager, A., T. Uchida, T. Maekawa, and M. Tachibana, Synthesis and characterization of Mono-disperse Carbon Quantum Dots from Fennel Seeds: Photoluminescence analysis using Machine Learning. *Sci. Rep.*, 2019. 9(1): p. 14004.

[143] Thakur, A., P. Devi, S. Saini, R. Jain, R. K. Sinha, and P. Kumar, Citrus limetta Organic Waste Recycled Carbon Nanolights: Photoelectro Catalytic, Sensing, and Biomedical Applications. *ACS Sustain. Chem. Eng.*, 2018. 7(1): p. 502-512.

[144] Campos-Vega, R., G. Loarca-Piña, H. A. Vergara-Castañeda, and B. D. Oomah, Spent coffee grounds: A review on current research and future prospects. *Trends Food Sci. Technol.*, 2015. 45(1): p. 24-36.

[145] Zhao, W., Y. Cui, X. Sun, H. Wang, and X. Teng, Corn stover biochar increased edible safety of spinach by reducing the migration of mercury from soil to spinach. *Sci. Total Environ.*, 2021. 758: p. 143883.

[146] Langer, M., M. Paloncýová, M. Medveď, M. Pykal, D. Nachtigallová, B. Shi, A. J. A. Aquino, H. Lischka, and M. Otyepka, Progress and challenges in understanding of photoluminescence properties of carbon dots based on theoretical computations. *Appl. Mater. Today*, 2021. 22.

[147] Ru, Y., G. I. N. Waterhouse, and S. Lu, Aggregation in carbon dots. *Aggregate*, 2022. 3(6).

[148] Ding, H., L.-W. Cheng, Y.-Y. Ma, J.-L. Kong, and H.-M. Xiong, Luminescent carbon quantum dots and their application in cell imaging. *New J. Chem.*, 2013. 37(8).

[149] Lu, S., Z. Li, X. Fu, Z. Xie, and M. Zheng, Carbon dots-based fluorescence and UV–vis absorption dual-modal sensors for Ag^+ and l-cysteine detection. *Dyes Pigm.*, 2021. 187.

[150] Wu, M., Y. Demissie, and E. Yan, Simulated impact of future biofuel production on water quality and water cycle dynamics in the Upper Mississippi river basin. *Biomass Bioenergy*, 2012. 41: p. 44-56.

[151] Grinstead, K. M., L. Rowe, C. M. Ensor, S. Joel, P. Daftarian, E. Dikici, J. M. Zingg, and S. Daunert, Red-Shifted Aequorin Variants Incorporating Non-Canonical Amino Acids: Applications in In Vivo Imaging. *PLoS One*, 2016. 11(7): p. e0158579.

[152] Zhang, Y., L. Pang, C. Ma, Q. Tu, R. Zhang, E. Saeed, A. E. Mahmoud, and J. Wang, Small molecule-initiated light-activated semiconducting polymer dots: an integrated nanoplatform for targeted photodynamic therapy and imaging of cancer cells. *Anal. Chem.*, 2014. 86(6): p. 3092-9.

[153] Ievtukhov, V., B. Zadykowicz, M. Y. Blazheyevskiy, and K. Krzyminski, New luminometric method for quantification of biological sulfur nucleophiles with the participation of 9-cyano-10-methylacridinium salt. *Lumin.*, 2022. 37(2): p. 208-219.

[154] Magalhães, C. M., J. C. G. Esteves da Silva, and L. Pinto da Silva, Study of coelenterazine luminescence: Electrostatic interactions as the controlling factor for efficient chemiexcitation. *J. Lumin.*, 2018. 199: p. 339-347.

[155] Haddock, S. H., M. A. Moline, and J. F. Case, Bioluminescence in the sea. *Ann. Rev. Mar. Sci.*, 2010. 2: p. 443-93.

[156].Magalhaes, C. M., J. C. G. Esteves da Silva, and L. Pinto da Silva, Comparative study of the chemiluminescence of coelenterazine, coelenterazine-e and Cypridina luciferin with an experimental and theoretical approach. *J. Photochem. Photobiol. B*, 2019. 190: p. 21-31.

[157] Magalhaes, C. M., J. C. Esteves da Silva, and L. Pinto da Silva, Chemiluminescence and Bioluminescence as an Excitation Source in the Photodynamic Therapy of Cancer: A Critical Review. *Chemphyschem*, 2016. 17(15): p. 2286-94.

[158] Magalhaes, C. M., J. C. G. Esteves da Silva, and L. Pinto da Silva, Tuning the Intramolecular Chemiexcitation of Neutral Dioxetanones by Interaction with Ionic Species. *Molecules*, 2022. 27(12).

[159] Pinto da Silva, L. and J. C. Esteves da Silva, Firefly chemiluminescence and bioluminescence: efficient generation of excited states. *Chemphyschem*, 2012. 13(9): p. 2257-62.

[160] Pinto da Silva, L., C. M. Magalhaes, D. M. A. Crista, and J. C. G. Esteves da Silva, Theoretical modulation of singlet/triplet chemiexcitation of chemiluminescent imidazopyrazinone dioxetanone via C(8)-substitution. *Photochem. Photobiol. Sci.*, 2017. 16(6): p. 897-907.

[161] Koo, J.-Y. and G. B. Schuster, Chemically initiated electron exchange luminescence. A new chemiluminescent reaction path for organic peroxides. *J. Am. Chem. Soc.*, 1977. 99(18): p. 6107-6109.

[162] Melhuish, W. H., Quantum Efficiencies of Fluorescence of Organic Substances: Effect of Solvent and Concentration of the Fluorescent Solute1. *J. Phys. Chem.*, 1961. 65(2): p. 229-235.